NASA CR- 160056

LMSC-D766177
AUGUST 1980

STUDY OF A SOLID HYDROGEN COOLER FOR SPACECRAFT INSTRUMENTS AND SENSORS

FINAL REPORT

FOR

NASA GODDARD SPACE FLIGHT CENTER

CONTRACT NAS 5-25792

DR. ALLAN SHERMAN, TECHNICAL OFFICER

APPLIED MATERIALS AND TECHNOLOGY LABORATORY

Lockheed

PALO ALTO RESEARCH LABORATORIES

LOCKHEED MISSILES & SPACE COMPANY INC • A SUBSIDIARY OF LOCKHEED CORPORATION
PALO ALTO CALIFORNIA

STUDY OF A SOLID HYDROGEN COOLER FOR SPACECRAFT INSTRUMENTS AND SENSORS FINAL REPORT AUGUST 1980

FOR NASA GODDARD SPACE FLIGHT CENTER
CONTRACT NAS 5-25792
DR. ALLAN SHERMAN, TECHNICAL OFFICER

APPLIED MATERIALS AND TECHNOLOGY LABORATORY
PALO ALTO RESEARCH LABORATORY
LOCKHEED MISSILES AND SPACE COMPANY, INC.
PALO ALTO, CALIFORNIA

CONTENTS

ILLUSTRATIONS

TABLES

Section 1
INTRODUCTION

The utilization of solid hydrogen in space for sensor and instrument cooling provides a very efficient technique, especially for long term cooling or for cooling at high heat rates. The solid hydrogen can provide temperatures as low as 7 - 8°K to instruments. In addition, when vapor cooling is properly utilized the single-stage solid hydrogen cooling becomes competitive with dual-stage coolers which are optimized and operated at higher temperatures utilizing higher temperature cryogens. The solid hydrogen can provide cooling of some instruments which would otherwise be cooled with helium in the absence of suitable solid hydrogen development. The use of solid hydrogen in place of helium leads to a weight reduction which may be as large as a factor of ten and an attendant reduction in system volume.

Although solid cryogen coolers have been utilized for long duration orbital instrument cooling in recent years, no solid hydrogen cooler development has been pursued for 15 years. This gap in solid hydrogen system development is primarily due to concerns about system safety which are undoubtedly magnified by the "Hindenburg Syndrome."

While liquid hydrogen and supercritical hydrogen have been utilized in space programs successfully, the utilization of solid hydrogen presents additional safety hazards due to the storage and operation of the hydrogen at absolute pressures of approximately 1/100 atmospheres. The potential for cryopumping of atmospheric gases into the container or plumbing lines exists if lines or joints are not vacuum-tight, and this requires special procedures and operations.

Hydrogen exists in two different molecular states; the para form in which the protons have opposing spins, and the more energetic ortho form which has uni-directional proton spins. At room temperature, normal hydrogen consists of approximately 25% para and 75% ortho, while at the normal boiling point temperature of 20.4°K, the mixture is greater than 99% para. The endothermic

conversion from mostly para to the equilibrium composition which is dependent upon temperature is an extremely slow reaction, taking hundreds of hours. However, use of appropriate catalysts can reduce the reaction time to fractions of a second. It is, therefore, possible to develop a catalytic converter which can be located in the hydrogen vent line and will use the endothermicity of the para to ortho conversion to enhance spacecraft instrument cooling with hydrogen.

This report presents the results of tests and studies to investigate the utilization of solid hydrogen for cooling of spacecraft instruments and sensors. The results are presented in two sections; the first describing the tests in which an existing single stage solid cooler was filled and tested with solid hydrogen and the second which describes the analysis and design of a catalytic converter which will be tested in the vent line of the cooler.

Section 2

SOLID HYDROGEN COOLER TESTING

2.1 DESCRIPTION OF TEST COOLER

The cooler which was utilized for the solid hydrogen testing is a flight back-up cooler similar to one utilized on a gamma ray experiment flown in orbit in 1972 aboard STP 72-2. [2-1] This cooler was flight qualified and has gone through both extensive thermal and vibration testing. It is a single stage unit designed for use with solid carbon dioxide. It has also been utilized recently (1976) for tests in which it was operated with solid neon for feasibility testing. In these tests it was operated at 17°K, which is close to the operating temperature with solid hydrogen.

The configuration of this cooler is shown in the drawing of Fig. 2-1. The general arrangement of the cooler along with the instrument module is shown in Fig. 2-2. The detector module was connected to the solid cooler by means of a shrink fit device and thermal link. Testing with the hydrogen took place with the instrument removed and the central cavity filled with a dexiglas rod as shown in the drawing. The flight cooler had a loaded weight of 48 lbs., which included 35 lb. of solid CO_2. The overall envelope is 16 in. long by 14 in. in diameter. The CO_2 was stored in an annular aluminum container supported by a fiberglass tube concentric with the system center line. This tank has a volume of 0.4 ft^3. The tube was made of 1581 glass cloth and Epon E-787 resin and varied in wall thickness from 0.07 in. to 0.09 in. A two-inch thick blanket of multilayer insulation (MLI) was applied by spirally wrapping on ten layers, goring the ends to provide a butt joint, and repeating the process on the next ten layers while staggering the gore joints so they did not align from one set of ten layers to the next. A total of 215 layers of each material was built up in this manner resulting in a total thickness of 1.9 in. A layer density of 113 layers/in. resulted.

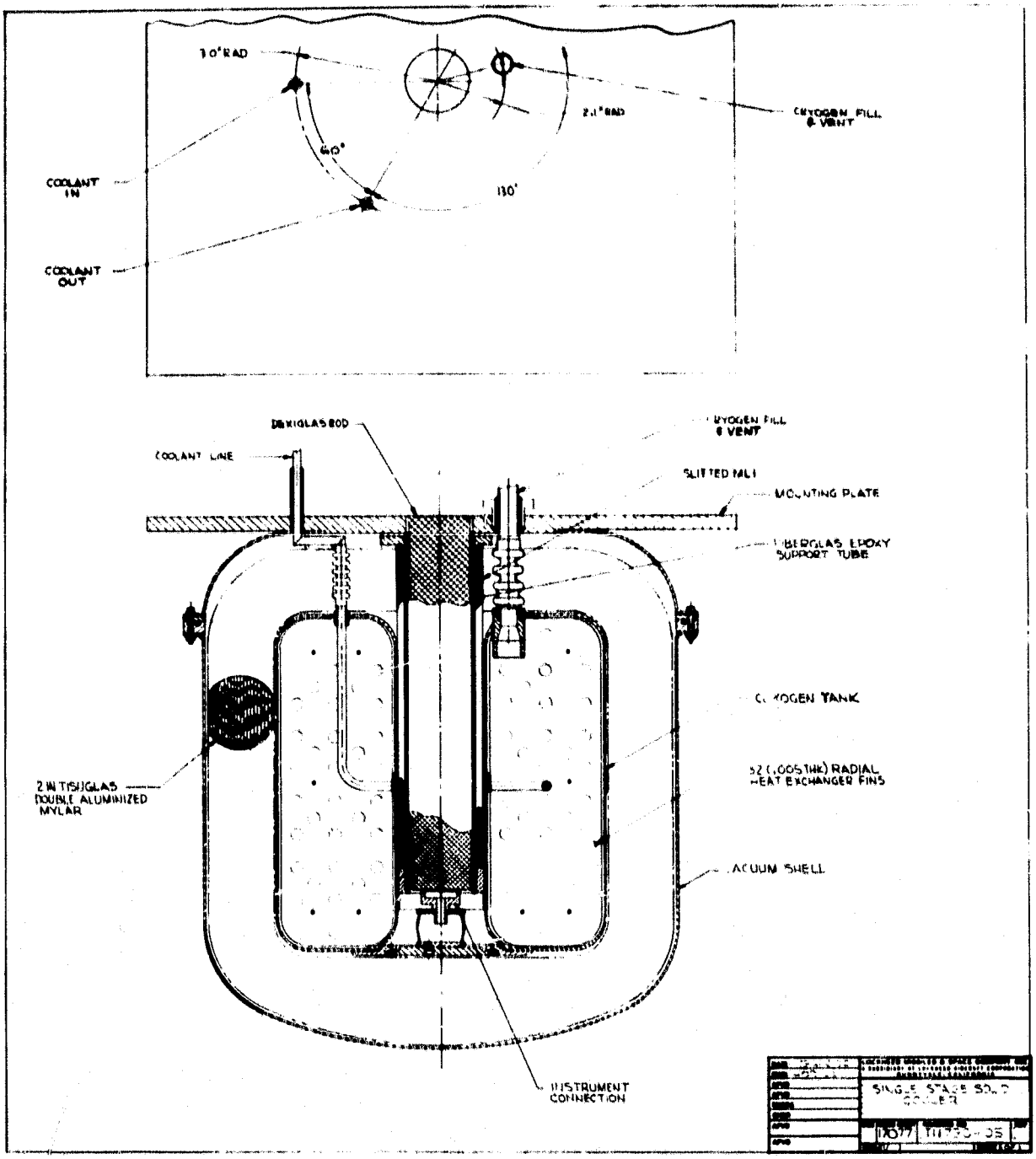

Fig. 2-1 Single Stage Solid Cooler

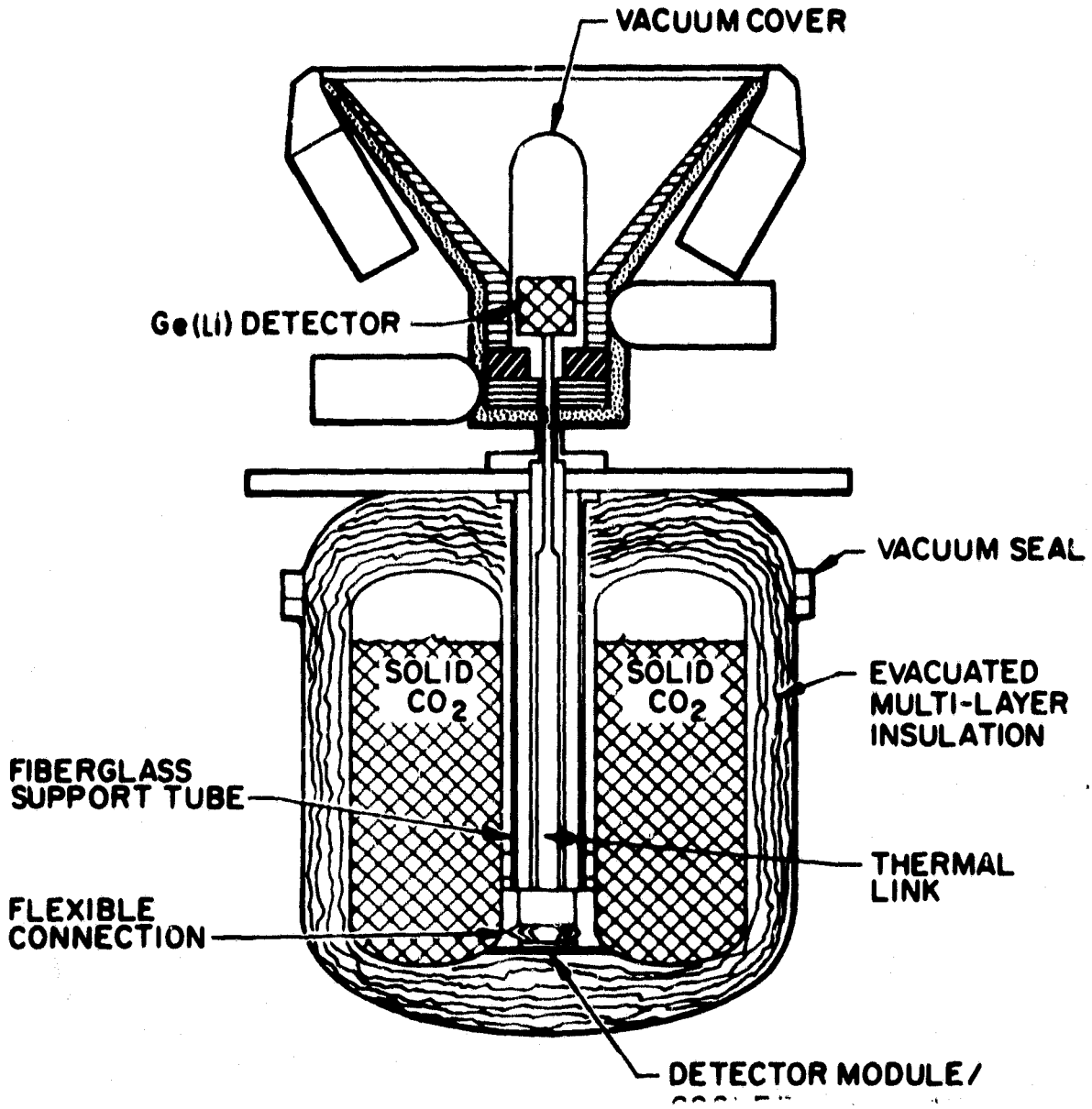

Fig. 2-2 General Arrangement of Cooler with γ-Ray Detector Instrument

Slitted MLI was wrapped around the fiberglas tube exterior to reduce radiative coupling in the annular space between the tube and CO_2 container and also to minimize heat flow from the fiberglass to the 1.9" MLI blanket. The slitting was performed to decrease conduction in the MLI parallel to the support tube.(2-2)

A finned copper heat exchanger inside the aluminum container was used to provide approximately uniform temperature during orbital lifetime as the cryogen was expended, and is shown in Fig. 2-3.

The plumbing lines into the container consist of a single line used for both venting and filling of the cryogen plus a cryogen inlet line and an outlet line used during filling and for periodic subcooling during spacecraft integration. These service lines were made of convoluted Teflon in order to minimize the heat leak to the system.

An external vacuum container was provided for the system, which was sealed at a flange with an O-ring seal.

2.2 TEST SET UP

The equipment shown schematically in Fig. 2-4 and photographically in Fig. 2-5 through 2-8 allows the following operations to be performed on the cryostat:

- o Evacuation and maintenance of cryostat's vacuum
- o Filling and subcooling of cryostat
- o Maintenance of cryogen at ~ 10K
- o Emptying the cryostat

2.2.1 Evacuation and maintenance of cryostat's vacuum -

A four inch liquid nitrogen cold trapped diffusion pump (DP) was used to evacuate and maintain pressure (< 1.0×10^{-5} Torr)

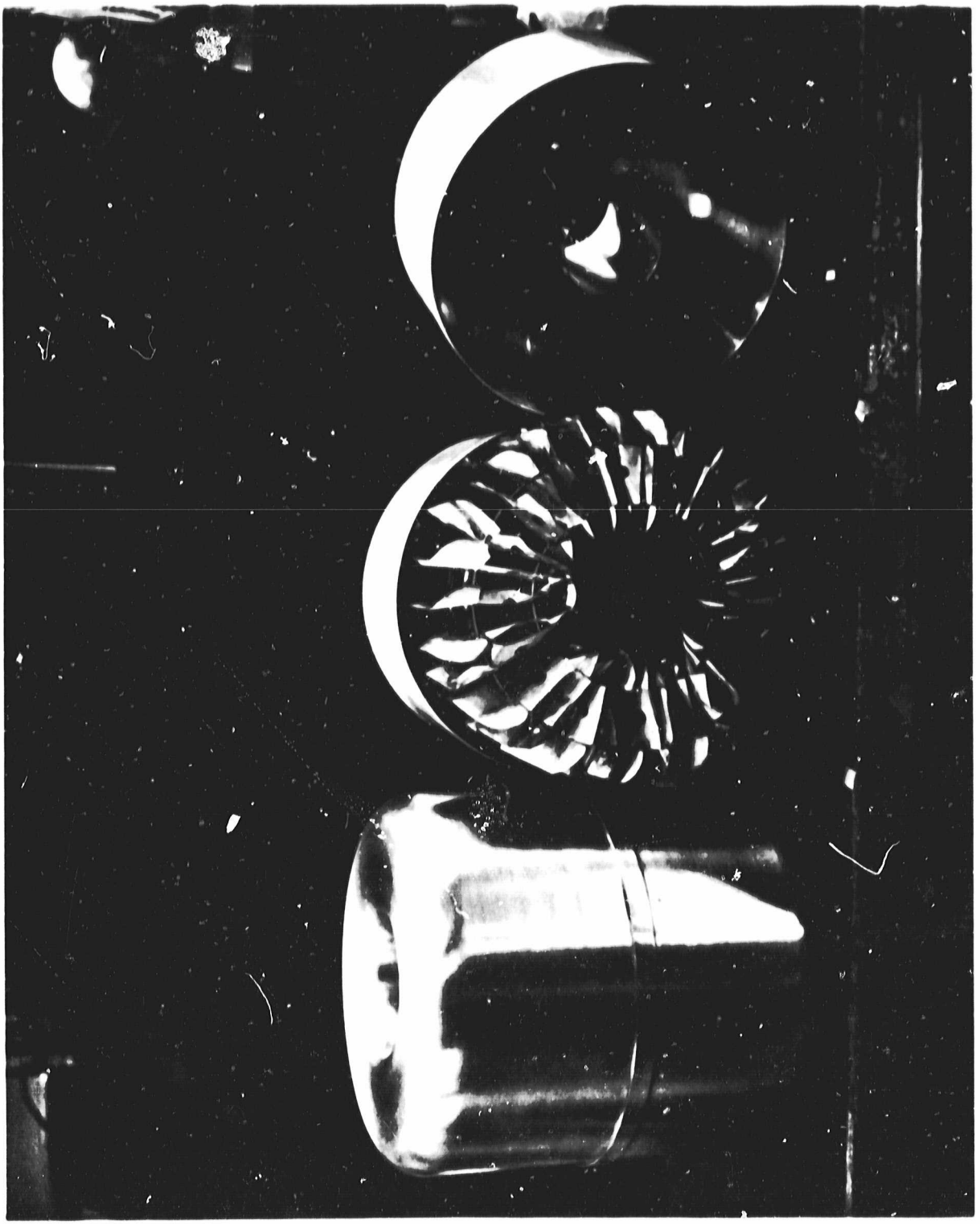

Fig. 2-3 Internal Heat Exchanger Configuration

SYMBOLS

V – MANUAL VALVE
AV – AUTOMATIC VALVE
RV – RELIEF VALVE
RP – ROUGHING PUMP
DP – DIFFUSION PUMP
CP – COLD TRAP
WTM – WET TEST METER
PG – PRESSURE GAUGE
SC – SWAGELOK CONNECTOR
QD – QUICK DISCONNECT
C – CRYOSTAT
TS – TEMPERATURE SENSOR
HE – HEAT EXCHANGER
PS – PURGE SHROUD
GHe – GASEOUS HELIUM
LN_2 – LIQUID NITROGEN
LHe – LIQUID HELIUM
LH_2 – LIQUID HYDROGEN
CT – CRYOGEN TANK
VT – CRYOGEN VENT
VM – VACUUM SPACE
CI – COOLING INLET
CO – COOLING OUTLET
FV – FACILITY VENT
CV – CALIBRATED VOLUME
VJ – HELIUM INLET VACUUM JACKET

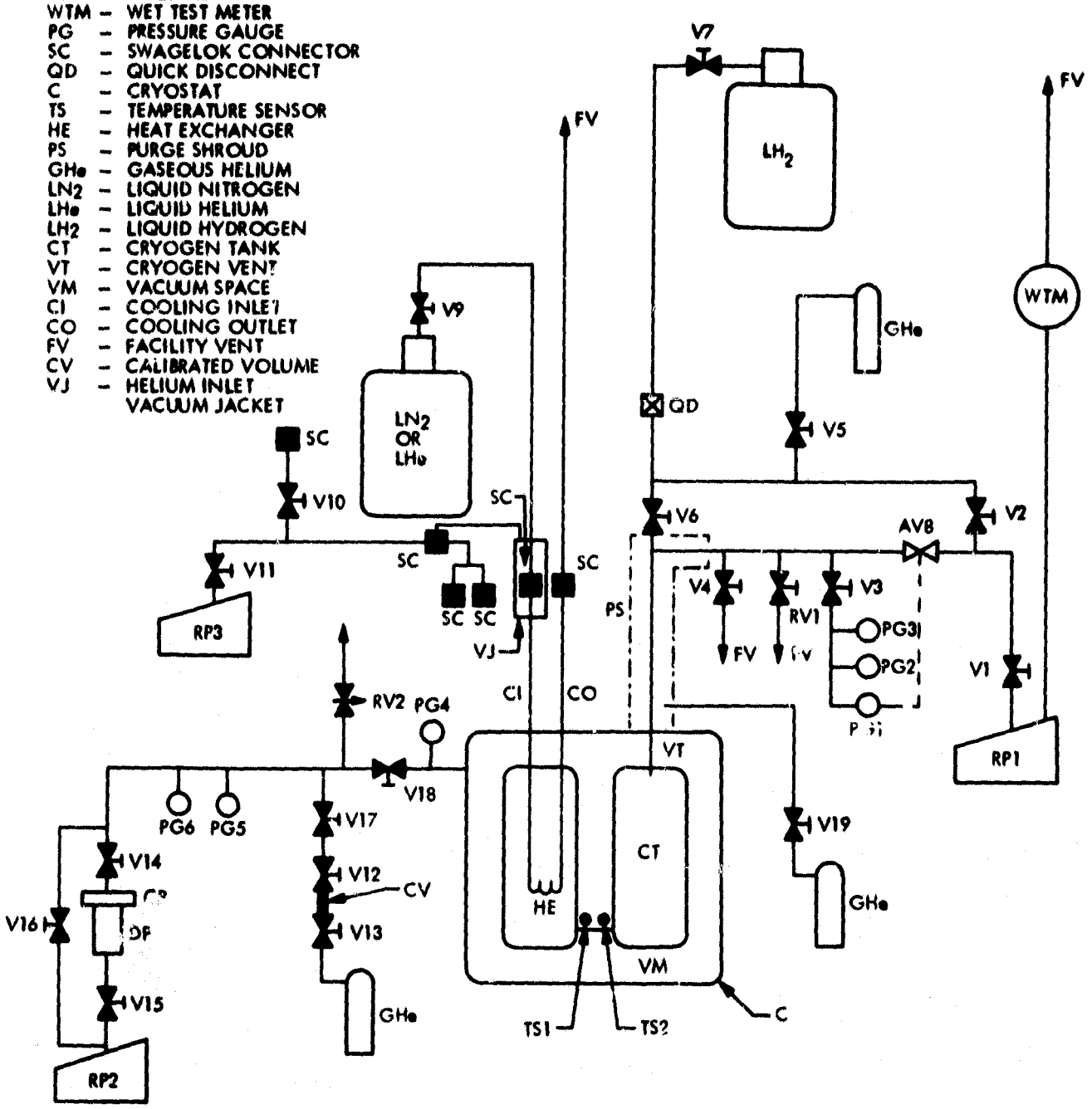

Figure 2-4. Solid Hydrogen Testing Schematic

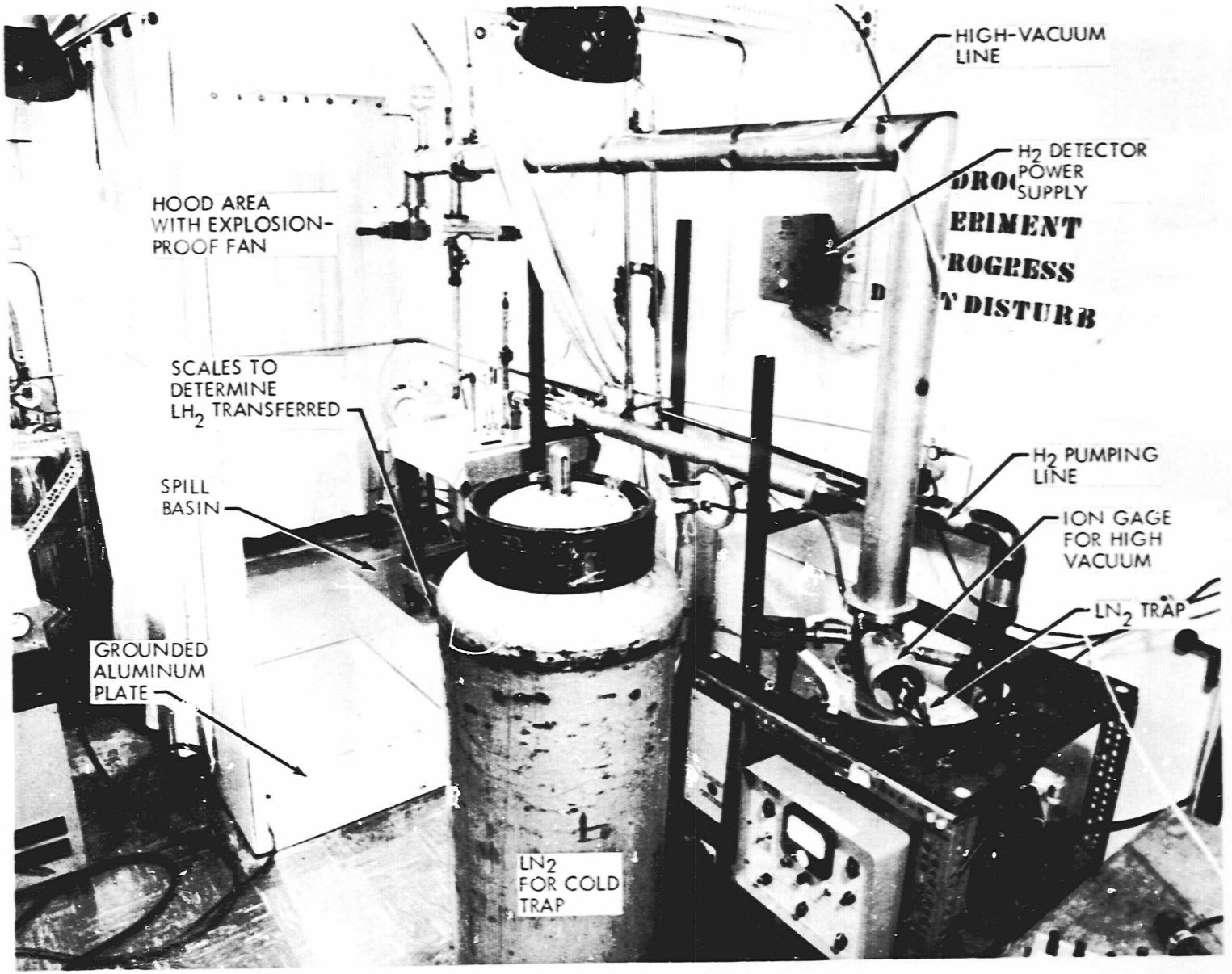

Fig. 2-5 Overall Test Set-up

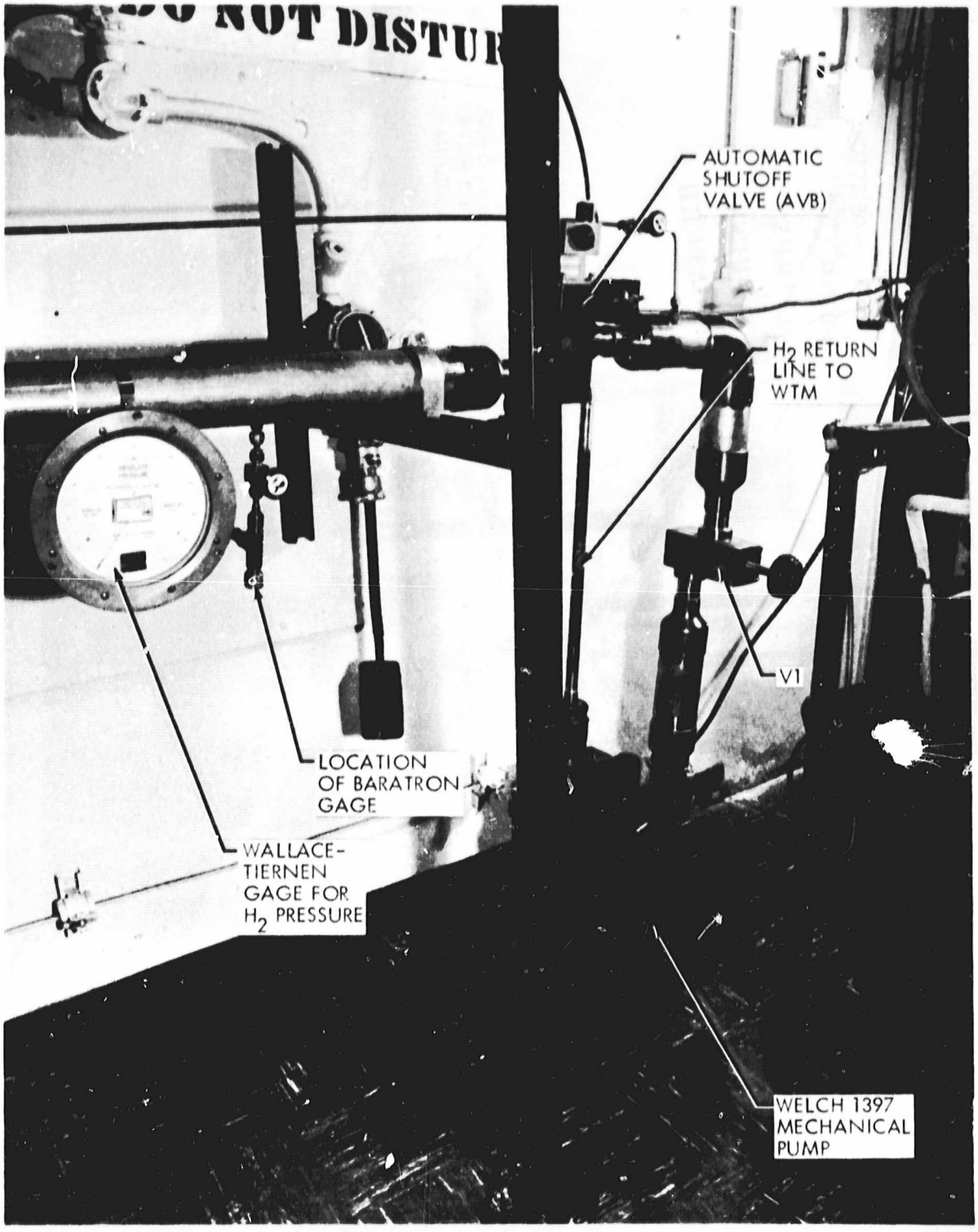

Fig. 2-6 H_2 Pump

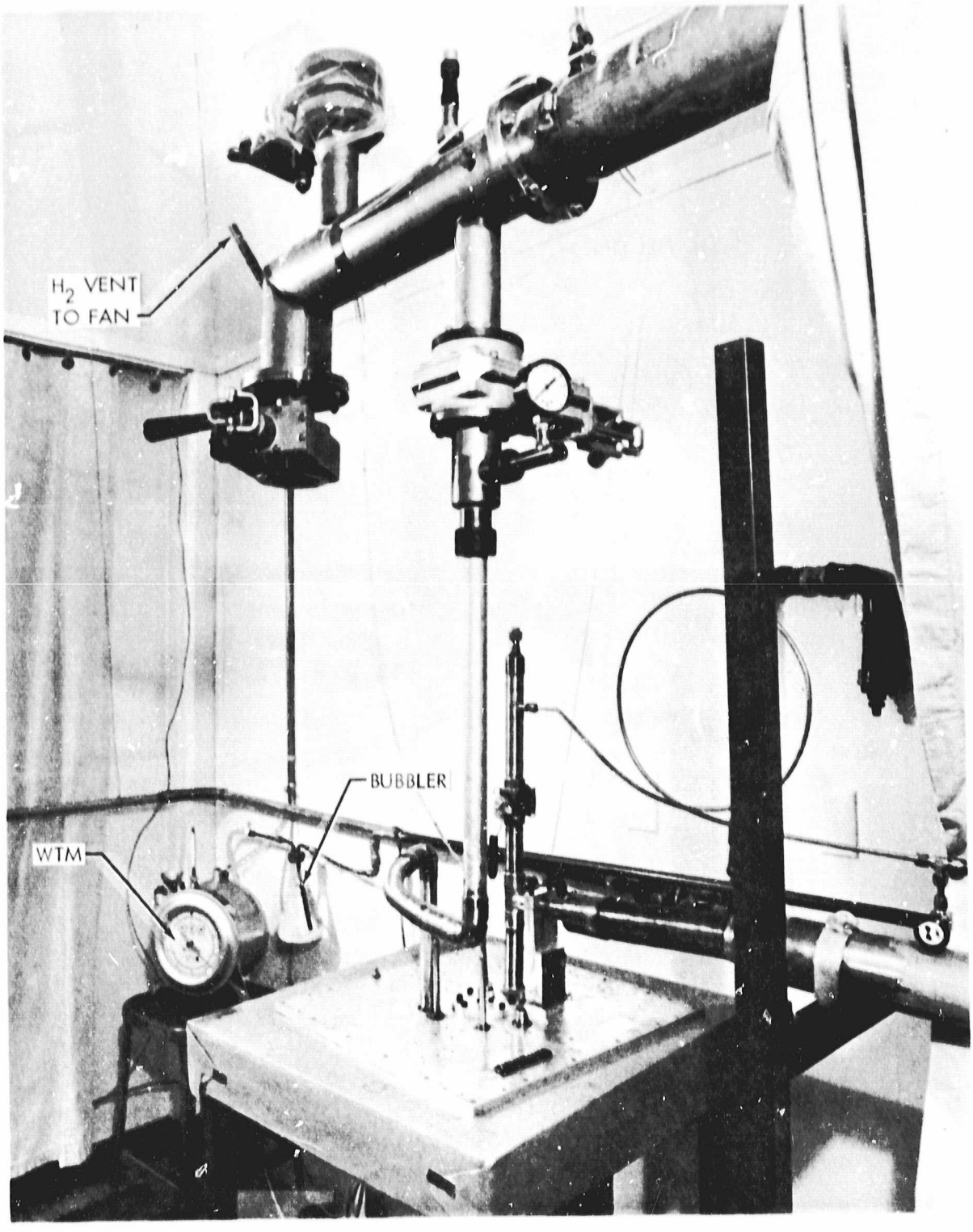

Fig. 2-7 Flow Metering System

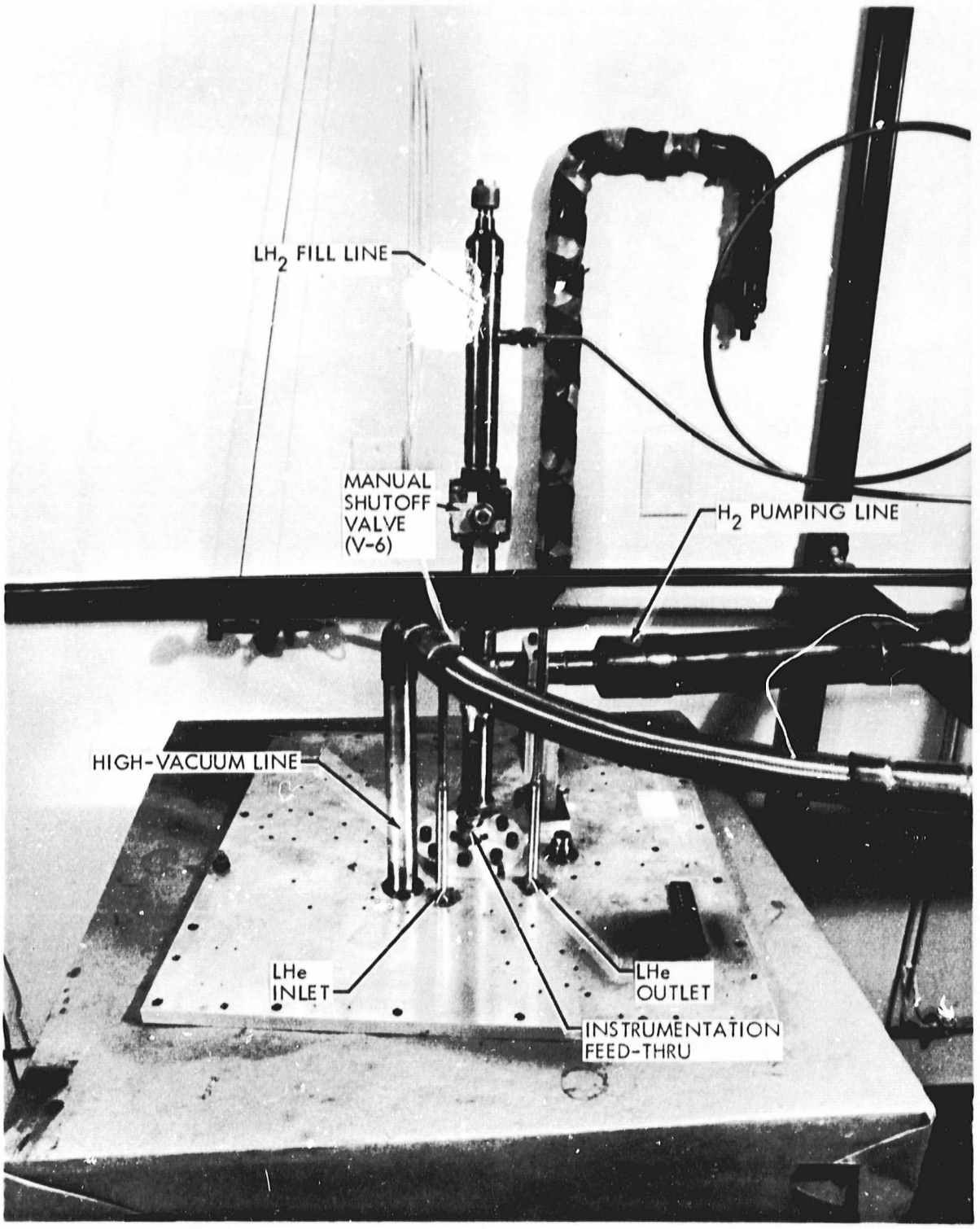

Fig. 2-8 Cryostat Top Plate

in the cryostat's vacuum space. This system is equipped with by-pass valving (V16,V15, V14) which allows initial rough down of the system using a Welch model 1402 roughing pump (RP2). Pressure measurements in the system are provided by a compound gauge (PG4), a thermocouple vacuum gauge (PG5), and an ionization gauge (PG6)

2.2.2 Filling and subcooling of cryostat - Filling of the cryostat with liquid hydrogen was achieved using a 165 liter supply of LH_2 and a vacuum jacket transfer line. Connection of the transfer line to the cryostat's plumbing is afforded through a quick disconnect and ball valve. During the fill, liquid air formation at the mounting plate is minimized using a helium pressurized shroud assembled around the cryostat's vent/fill line at the mounting plate.

Subcooling the cryogen was achieved using a 100 liter supply of liquid helium,a vacuum jacketed transfer line, and vacuum jacket assembly placed around the helium inlet swagelok. Following the subcooling operation, a vacuum is maintained in the cryostat coolant line using roughing pump (RP3).

2.2.3 Pumping system for hydrogen - Pumping on the hydrogen to maintain it as a solid at < 10K was achieved in this testing using a Welch model 1397 roughing pump and a 4" pumping line. The vent side of the 1397 pump is coupled to a wet test meter so that cryogen flow rates can be monitored. Cryogen vapor pressure measurements were afforded using an MKS baratron (PG1) sensitive in the 0 to 10 Torr range. The baratron concept allows pressure measurements without the use of a hot filament. Vent line protection from the cryopumping of oil in case of a pump failure is achieved in the vent system using pneumatic valve AV8 and a relay in the baratron's controller. Valve AV8 is closed automatically if there is a pressure rise in the system so that PG1 reads above a certain pre-set value.

In addition to the baratron pressure gauge, the hydrogen vent line is equipped with a 0 to 5 Torr Wallace and Tiernan gage (PG3) and a compound pressure gauge (PG2). Emergency pressure relief in the hydrogen vent line was provided with a 10 PSIG relief valve (RV1).

2.2.4 Emptying the Cryostat. Valves V13, V12, and V17, along with a "calibrated volume" were used to introduce helium into the cryostat's vacuum space. The introduction of the helium raises the heat flux into the cryogen thereby speeding the emptying process.

2.3 TEST RESULTS

2.3.1 Checkout testing. Prior to testing with hydrogen the following checkout tests were run:

a) Fill with LN_2 followed by pumping on LN_2 to solid and determination of steady state conditions, followed by cooler emptying procedure.
b) Circulation of LHe through the coolant coils without cryogen in tank.
c) Fill with LHe and allow helium to boil-off and vent at atmospheric pressure.

In test a) with LN_2 the steady state temperature corresponding to the measured vapor pressure of 0.27 Torr was 44K, which was in good agreement with predictions for the system operation. The temperature sensor was separated from the tank by a bolted-indium filled joint and indicated $47^{o}K$ which we feel resulted from a temperature difference across the joint.

The heat rate corresponding to the flow rate of 0.2 ft^3/hr was 487 mW which was approximately 50% above the expected value of 320 mW. The cause of this is not known, however, it was speculated that the insulation pressure may have been high enough for a

significant gas conduction contribution. The pumping system pressure was 1.5×10^{-7} Torr, however, the pressure at the cooler was not measured.

In test b) circulation of LHe through the coolant coils was performed without incident. In test (c) the helium boil-off was sufficient to cause a small amount of liquid air formation (several drops) on the un-insulated line near the cooler. This was considered undesirable during the hydrogen testing, so a purge box which would utilize helium purge gas during testing was constructed to be used during the hydrogen tests. It was initially intended to provide a closed cell foam insulation around the line, however, we were concerned that the insulation might allow areas of the line which utilized rubber O-rings for vacuum sealing to freeze and cause vacuum leaks.

These tests served to check out the system operation and to evaluate the test procedures which were written prior to testing with hydrogen.

2.3.2 Hydrogen testing - Two tests were conducted with hydrogen. The following chronolog indicates the significant events for the first of these two tests. Difficulty was encountered in the first test when after filling the tank with LH_2, the coolant loop for the LHe circulation evidently froze up with condensibles during helium cooling. The hydrogen was subsequently frozen by vacuum pumping; a process which required about one hour.

Figs. 2-9 and 2-10 show the vapor pressure history and flow rate history and indicate the significant events during these tests. The tank was filled with 1.48 lbs. of LH_2. This is 85% of its capacity. After the liquid was frozen by pumping, it was decided to do a partial warm-up of the cooler by letting a

SH_2 TEST NO. 1

CHRONOLOG

DATE	TIME	EVENT
3-25-80	1310	Begin LN_2 cooling of tank
	1556	Discontinue LN_2 cooling
	1603	Begin pumping on coolant line
	1610	Begin LH_2 transfer
	1617	Stop LH_2 transfer
	1655	Attempt to start liquid helium cooling of cryogen
	1701	Evacuate coolant line. Line is plugged.
	1730	Begin pumping on cryogen
	1755	Cryogen at triple point ~ 54 to55^{o}K
	1823	Cryogen pressure begins to drop below triple point
	1900	WTM Total - 45.1 Ft^3 PG1 1.5 Torr
3-26-80	0930	Instantaneous flow rate = 1.1 Ft^3/Hr WTM Total -65.2 Ft^3
	0940	Begin Emptying Process. Begin to let helium gas into vacuum space.
	1200	Instantaneous flow rate = 9.0 Ft^3/Hr, WTM Total - 89.1 Ft^3
	1423	Discontinue emptying process. Pump out helium gas WTM Total - 113.3 Ft^3
3-27-80	1518	Performing heat rate test WTM,Total = 139.83 Ft^3
		3 hour flow rate = 1.16 Ft^3/Hour
		PG1 pressure with V1 Closed = 1.1 Torr

DATE	TIME	EVENT
3-28-80	1056	Performing heat rate test.
		WTM Total - 162.67 Ft^3
		15 Hour Flow Rate = 1.17 Ft^3/Hr
		PG1 Pressure with V1 Closed = 1.0 Torr
	1445	Begin to empty cryostat
	1530	Flow rate = 10 Ft^3/Hr
		@ 37 μ He in vacuum space
	2100	Flow Rate = 10 Ft^3/Hr.
		@ 70 μ He in Vacuum Space
3-29-80	0040	Flow Rate = 0.0
		WTM Total = 263.95 Ft^3
		CRYOSTAT EMPTY

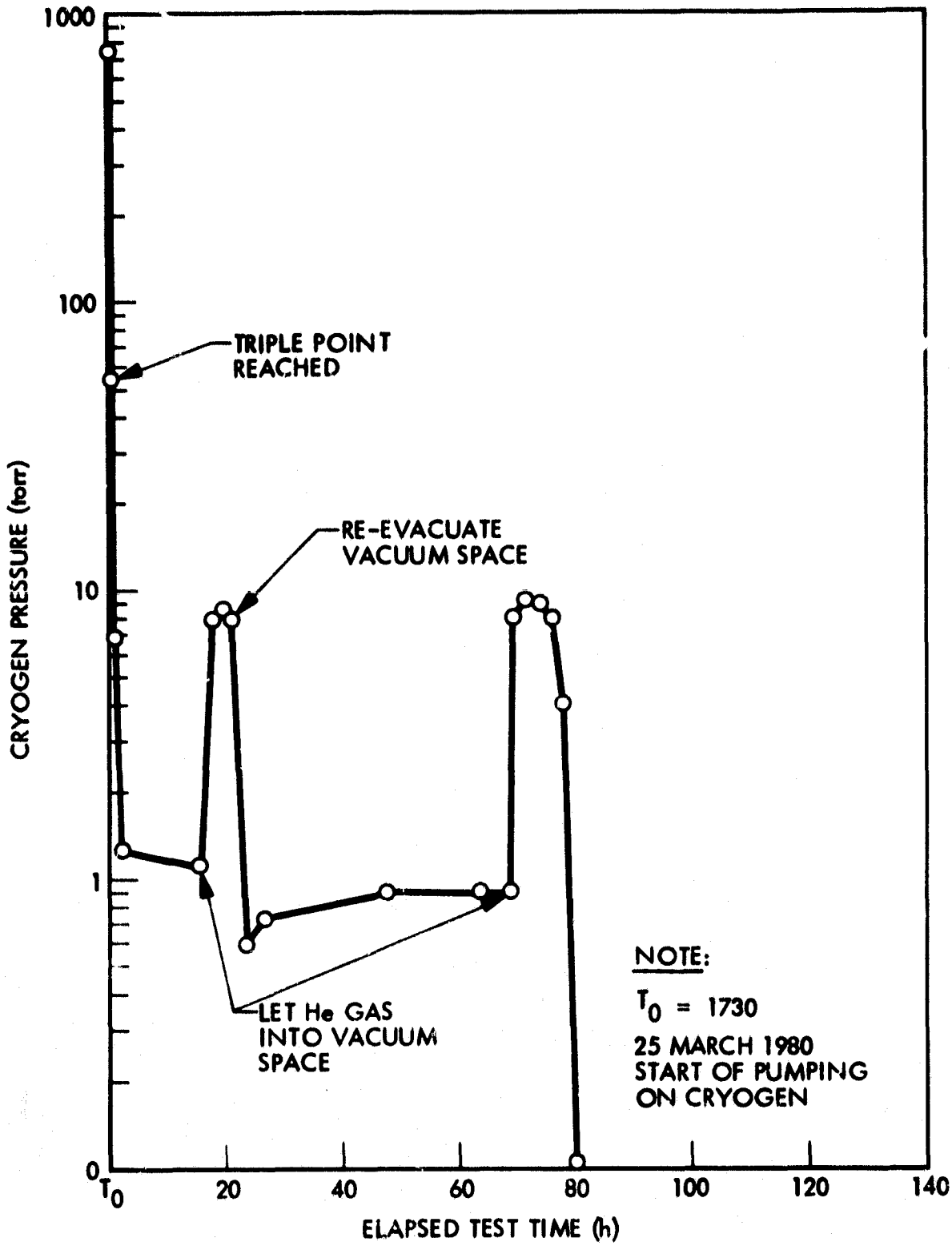

Figure 2-9 Cryogen Vapor Pressure vs. Time, Test No. 1

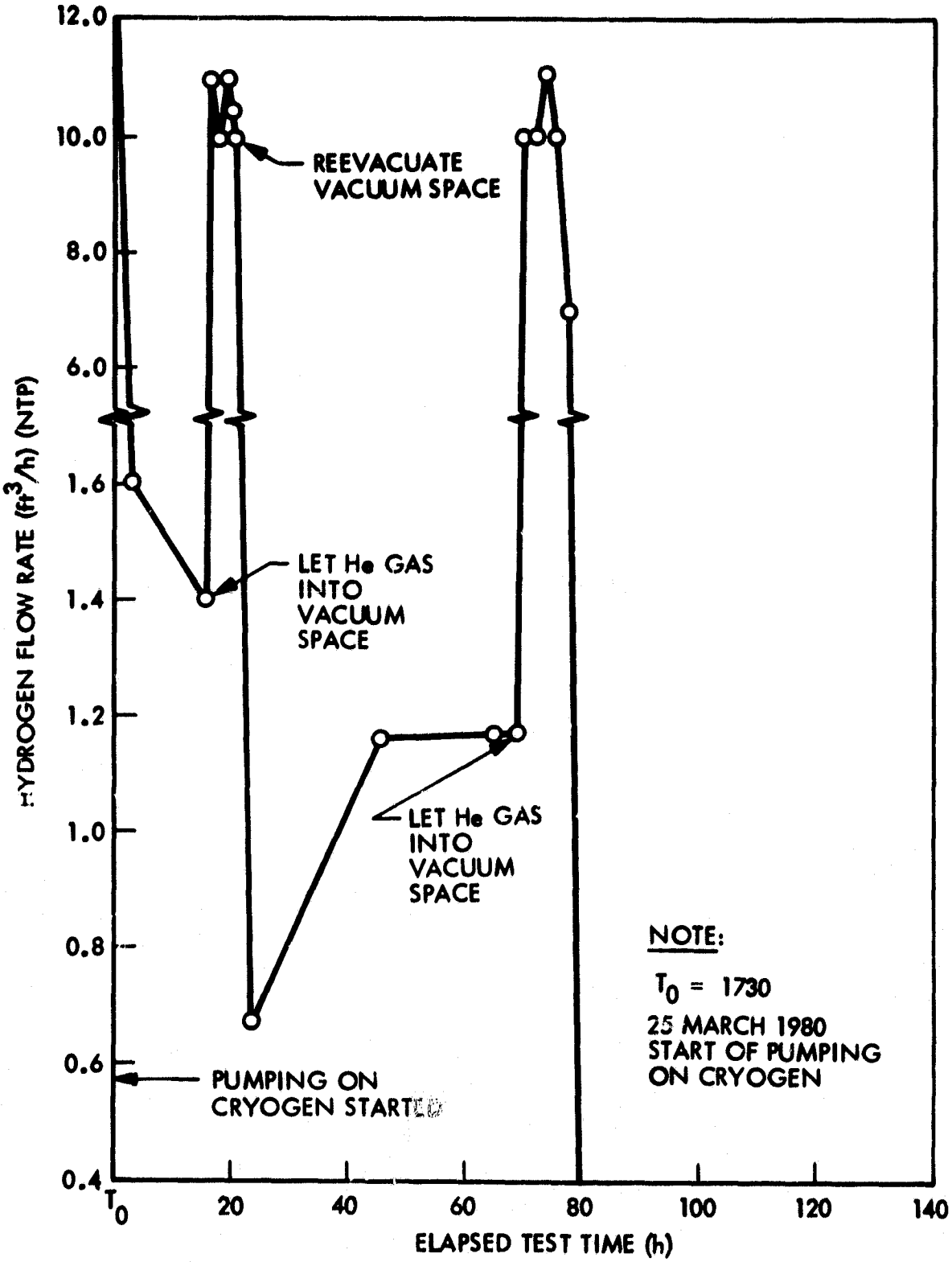

Figure 2-10 Cryogen Flow Rate vs Time, Test No. 1

small quantity of helium into the insulation space. The insulation pressure was let up to 20 microns pressure and the flow rate increased to approximately 10 ft^3/hr flow. The system was maintained at this condition for about 5 hours without incident. At this time it was decided to re-evacuate the insulation space and allow the hydrogen to attain steady state heat rates and temperature. This was accomplished and the system was allowed to pump for approximately two additional days when it was evident that both heat rates and temperatures were at steady state at values which were close to predicted levels.

At that point the system was emptied by letting 20μ of helium gas into the insulation space while continuing to pump on the hydrogen so that it remained in solid-vapor equilibrium during the emptying process. The flow rates during this process were approximately 10 Ft^3/Hr, as before, and the line pressure increased to approxiamtely 10 Torr as shown on Fig. 2-9. The steady state values for this test were 1.17 Ft^3/Hr and 1.1 Torr vapor pressure with the valve to the mechanical pump closed. These values correspond to a heat rate of 385 mW and a hydrogen temperature of 9.6°K which, as will be shown, are in excellent agreement with predicted values.

For the second test the procedure for purging and attaching the liquid helium supply to the coolant line was modified to preclude possible cryopumping of condensibles into the coolant loop.

The procedure which evolved and which was utilized for this test is presented in Appendix A.

The test chronolog is summarized on the following pages.

SH_2 TEST NO. 2

CHRONOLOG

DATE	TIME	EVENT
4-2-80	1041	Begin LN_2 cooling of tank
	1348	Discontinue LN_2 cooling
	1356	Begin coolant line purge and pressurization
	1407	Begin LH_2 transfer
	1409	Stop LH_2 transfer
	1521	Begin LHe cooling
	1546	Begin pumping on cryogen to ensure open line P = 10" Hg.
	1549	Discontinue pumping. $2Ft^3$ removed. P = 15" Hg.
	1637	Triple point of cryogen reached (54 torr)
	1652	Triple point breakthrough pressure ~ 2 torr
	1724	Discontinue LHe cooling
	1726	Disconnect LHe line and begin pumping on coolant coil
	1727	Open valve V1 and begin pumping on solid hydrogen
4-3-80	1741	Performing heat rate test. WTM Total = $31.04\ Ft^3$ 24 Hour flow rate = $1.23\ Ft^3/hr$
4-4-80	1510	Performing heat rate test WTM total = $57.72\ Ft^3$ 24 hour flow rate = $1.23\ Ft^3/hr$

DATE	TIME	EVENT
4-5-80	1520	Performing heat rate test
		WTM Total - 87.44 Ft^3
		24 hour flow rate = 1.23 Ft^3/Hr
4-6-80	1500	Performing Heat Rate Test
		WTM Total - 115.83 Ft^3
		24 hour flow rate = 1.20 Ft^3/Hr
4-7-80	0830	Close V1 and record PG1 pressure
		PG1 - 1.1 Torr
4-7-80	1539	Performing Heat Rate Test
		WTM Total - 144.68
		24 HOUR FLOW RATE = 1.17 FT^3/Hr
4-8-80	0855	Performing Heat Rate Test
		WTM Total - 164.22
		16 HOUR FLOW RATE = 0.96 FT^3/HR
		FLOW RATE AND PRESSURE DROPPING RAPIDLY.
		PROCEED TO EMPTYING PROCEDURE
	0905	Let Helium Gas into vacuum space
	0917	Flow Rate - 3.0 Ft^3
		with He pressure at 50μ
	0925	Close V1 and let remainder of cryogen warm
	0935	Pressure rose immediately to 18.0 in Hg and then stopped.
	0945	Open valve V1 and evacuate tank. PG1 pressure dropped to 0.00 indicating an empty tank.

The flow rate and pressure histories are given in Figs. 2-11 and 2-12.

In this test the cryogen tank was filled to only 54 % of its capacity due to difficulties with the scales. The measurement of 1 lb. changes for a 85 lbs system requires exacting procedures, and events such as thermal contraction of transfer lines or contraction of bellows due to pressure changes can lead to significant errors.

After the fill the liquid hydrogen was cooled by LHe circulation through the coils without incident. Freezing and subcooling of the hydrogen required only two hours and consumed 8 lbs. of LHe. During the freezing process it was attempted to achieve efficient cooling by limiting the helium flow rate to approximately 2-3 lbs/hr, a flow estimated from a prior study to utilize the helium efficiently. If the heat of vaporization of the helium is used (no vapor cooling), calculations indicate that 5.9 lbs of LHe are required to cool one lb of hydrogen from its NBP to triple point liquid - freeze it and further cool the solid to $9^{o}K$. The actual usage was 8 lbs. He/ .93 lbs H_2 = 8.6 which is very close to the minimum utilizing the heat of vaporization only.

Cooling was continued until the hydrogen vapor pressure dropped to 0.6 Torr corresponding to a temperature of 9.0K at which point LHe cooling was stopped and pumping on the solid hydrogen was started. Pumping was continued for 5½ days at which time the emptying process was initiated. As Figs. 2-11 and 2-12 show, the flow rate was starting to drop and the vapor pressure was dropping slightly at that time.

As the procedure indicates, it was intended to investigate a new emptying technique. In this method the insulation space was

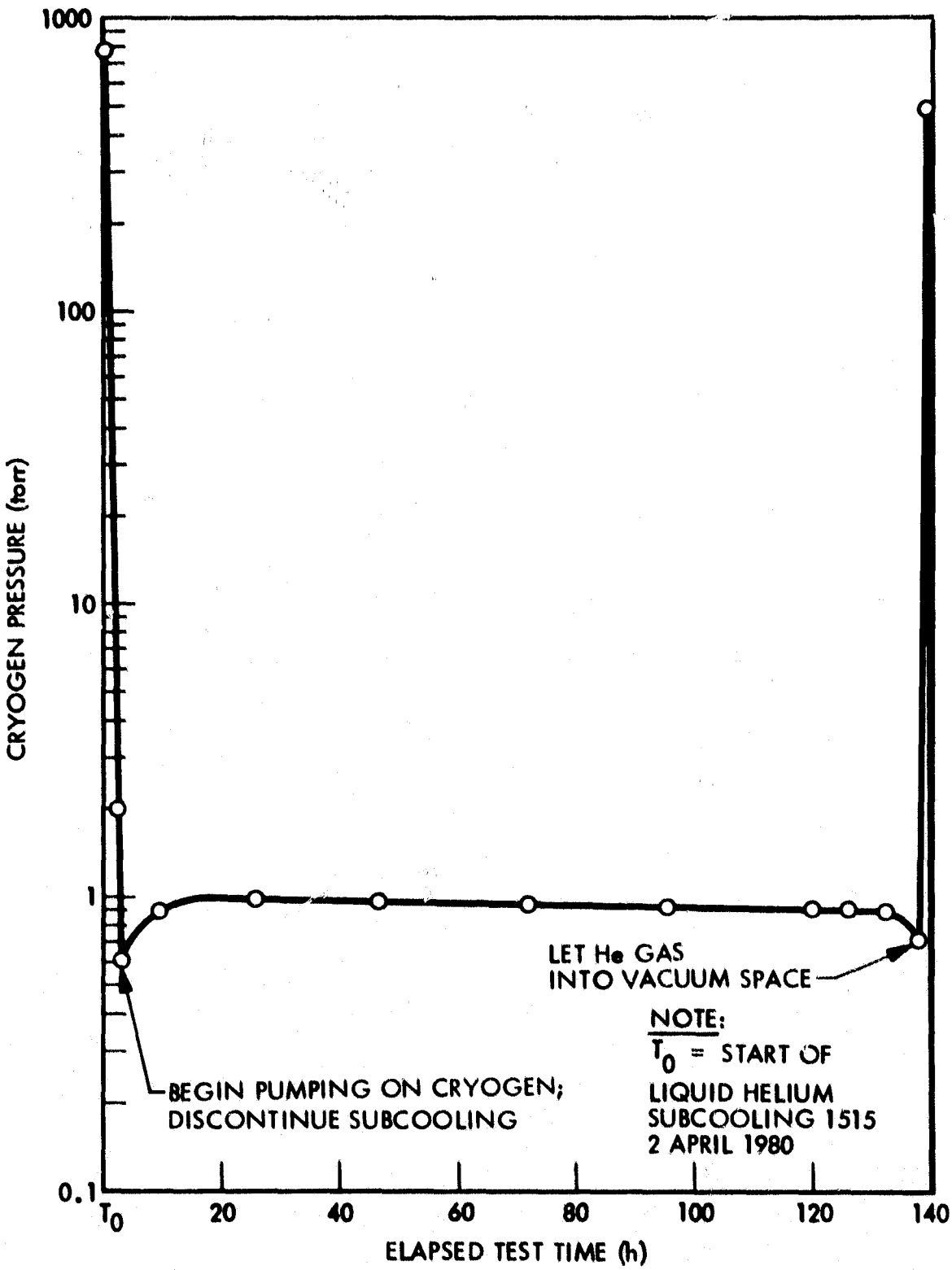

Figure 2-11 Cryogen Vapor Pressure vs. Time, Test No. 2

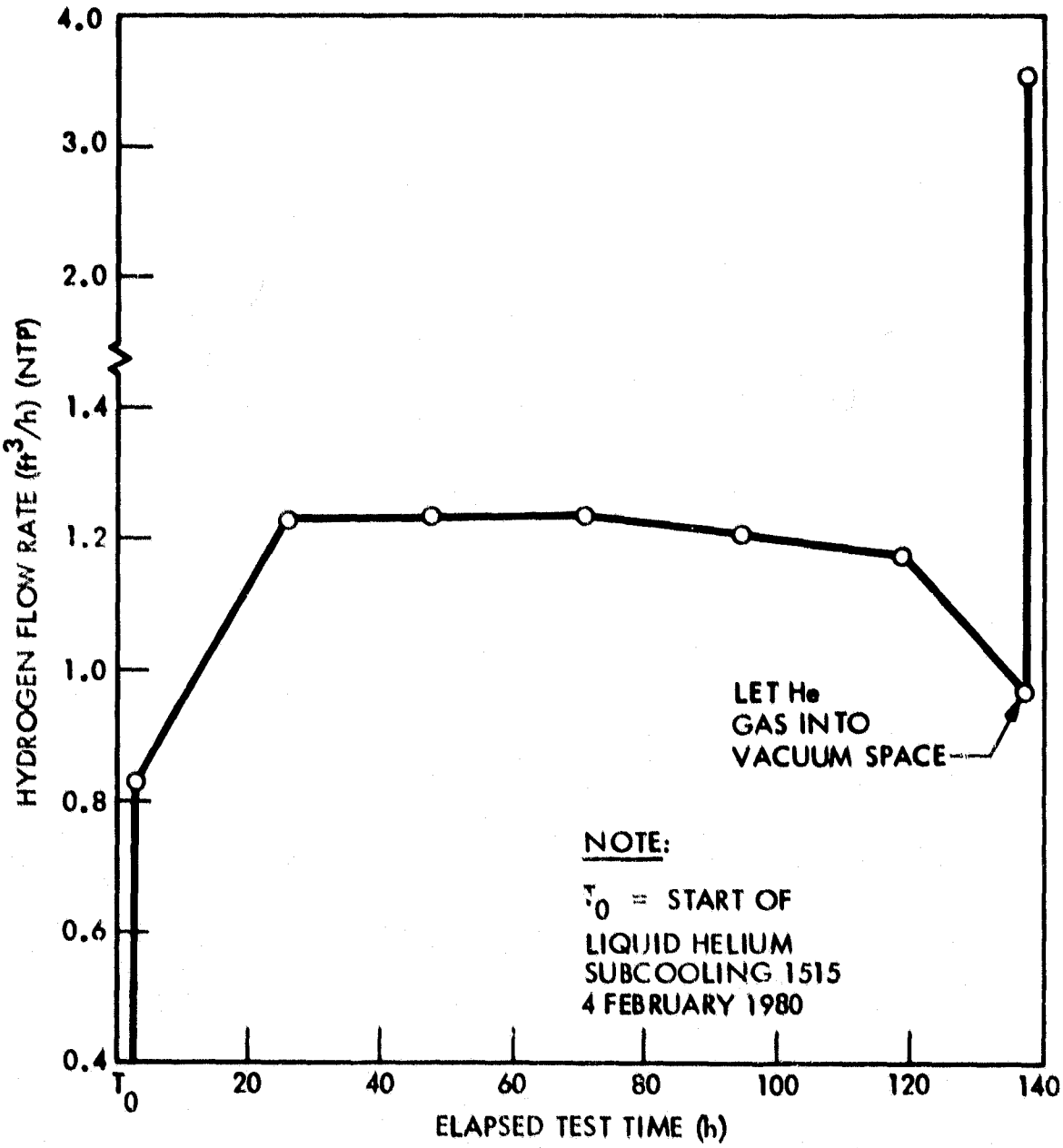

Figure 2-12. Cryogen Flow Rate vs Time, Test No. 2

let up with 20 microns of He gas as before while pumping on the vent line. After the expected high flow rates were established, the pumping was to be discontinued and the solid allowed to liquefy and warm to atmospheric pressure. At this point, the LH_2 would be allowed to vent at normal boiling point until empty.

This procedure was started, however, shortly after letting up the insulation space with He gas the pressure rose to 18" Hg (vacuum) and remained constant indicating the tank was empty. The tank was then evacuated by pumping and the test was terminated. The premature emptying of the tank was caused by the erroneous scale readings previously described.

2.4 PREDICTED PERFORMANCE AND CORRELATION

2.4.1 Heat Rates Heat rate predictions were made with a thermal analyzer computer program. The configuration was divided into nodes, and the program used a finite difference solution for the three dimensional heat transfer equation at each node. The program incorporated temperature-dependent material properties. The final computer output consisted of the temperatures of all nodes and heat rates for specified nodes.

The effective MLI conductivity used in the analysis was based on data obtained from tests made in the Lockheed Research Laboratories with a tank calorimeter of approximately the same shape and size as the CO_2 cooler.[2-3] This calorimeter was designed to reduce other heat loads (supports, plumbing) to approximately 10% of the total, yielding a highly accurate measure of the MLI heat leak.

The MLI conductivity expressions which were obtained previously [2-4] by flat plate calorimetry were modified by the tank calorimeter results and the resulting equations were used. The average effective MLI conductivity was 3.64×10^{-7} w/cm^{o}K (2.1×10^{-5} BTU/HR-FT^{o}R) for the solid H_2 temperatures (10K). The fiberglass conductivity was taken from measured data at LMSC.[2-5]

Table 2-1 presents a summary of previous correlations between test and predictions as well as the comparison for the solid hydrogen tests. The measured value of 385 mW compares favorably with the predicted value for the solid H_2. The test results are 5% higher than predicted.

2.4.2 Operating temperatures/pressures - The operating temperature of the system depends upon the pressure drop in the pumping system and the cryogen flow rate which depends upon the heat rate. Preliminary predictions were made for the pressure drop in the system during the preparation of the proposal. The predictions were based on the measured heat rate (339 mW) from a prior test utilizing solid neon and the preliminary pumping system design.

The pressure as a function of the pumping speed from the proposal is shown in Fig. 2-13. The pressure drop calculations were conducted utilizing a computer program based on Pouiselle flow. The predicted pressure at the pump was obtained from the pumping speed curves from the manufacturer shown in Fig. 2-14.

Both the pressure at the pump and the cryogen pressure are shown on the figure. The predicted pressure drop in the line is small, on the order of 0.2 Torr. With the Welch 1397 mechanical pump which was utilized for the tests the predicted pressure over the cryogen is 1.1 Torr. The test data are shown on the curve.

Table 2-1

COMPARISON OF MEASURED AND PREDICTED COOLER HEAT RATES

Heat Load Source*	With CO_2 at 125 K		With Neon at 17 K		With Hydrogen at 10 K	
	Predicted (mW)	Measured (mW)	Predicted (mW)	Measured (mW)	Predicted (mW)	Measured (mW)
Multilayer Insulation						
• Around Tank	101		119		119	
• Between Support Tube and Tank	35		38		38	
Fiberglas Support Tube	132		183		184	
Plumbing Lines	14		24		24	
Total Load	282	288	364	339	365	385

*Hot Boundary at 300 K

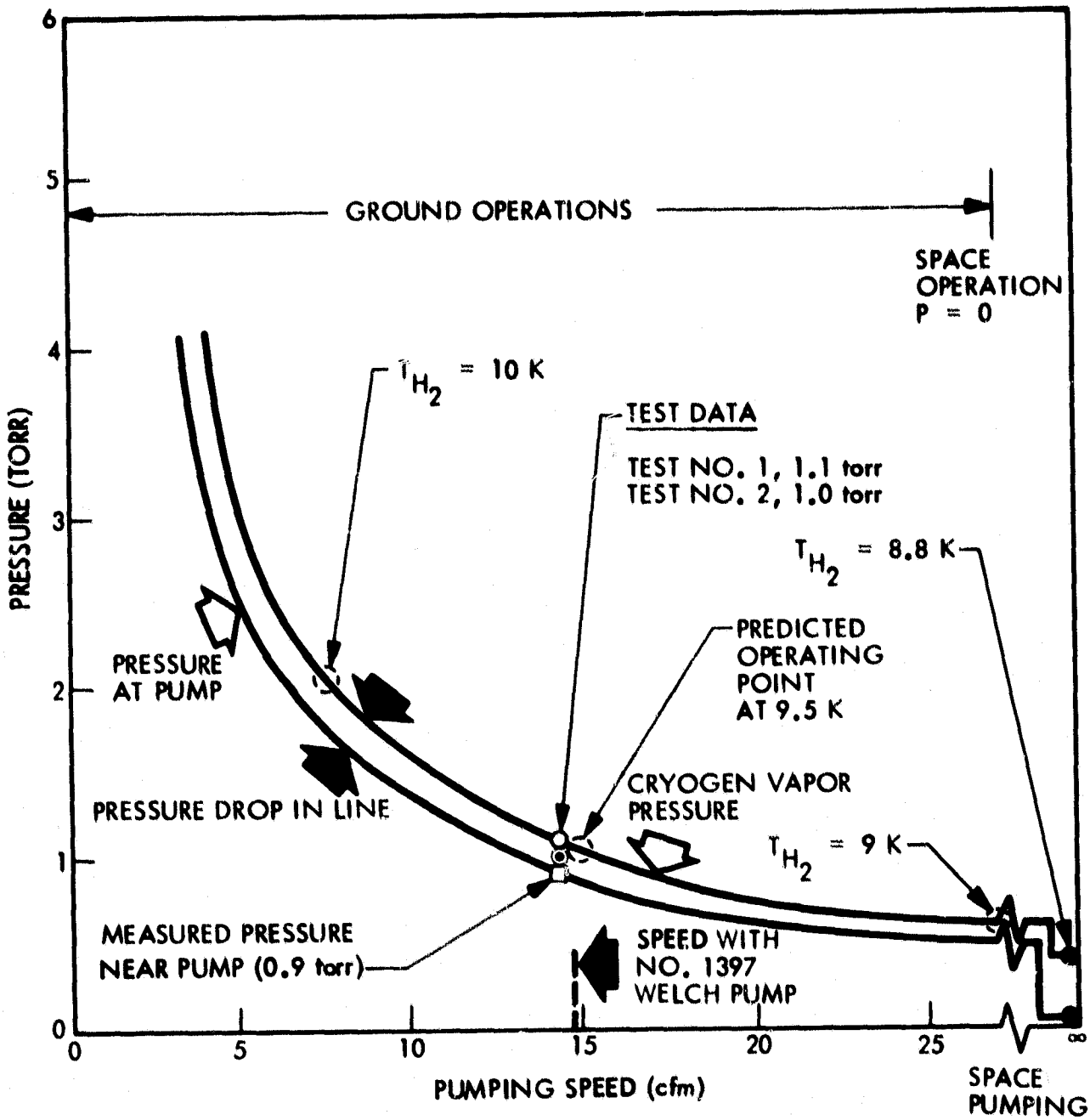

Figure 2-13 Effect of Pumping Speed on Cryogen Pressure and Temperature

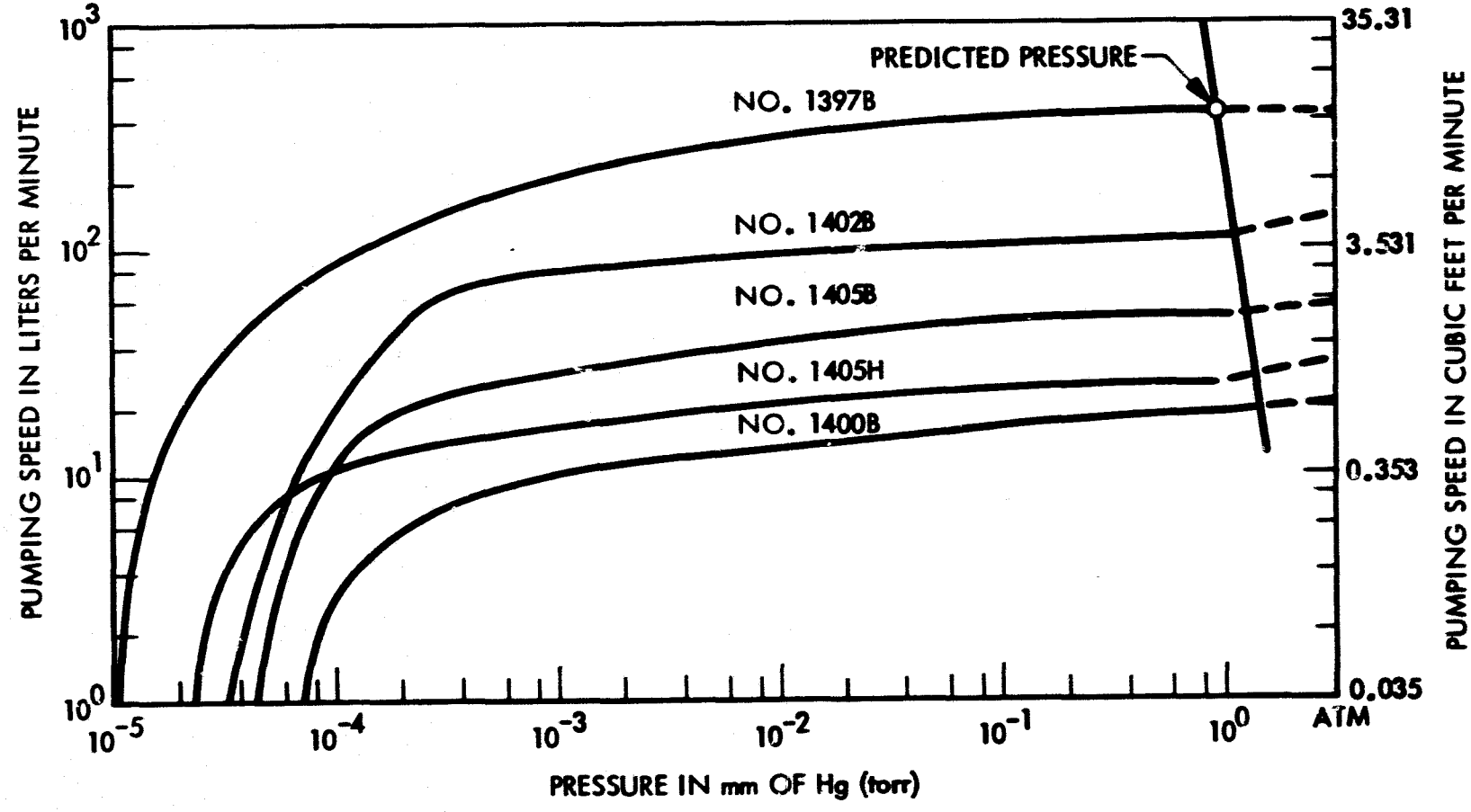

Figure 2-14 Performance Curves for Welch Pumps

The measured pressure near the pump was 0.9 Torr and the measured pressure with the pump valved off was 1.1 Torr for test No. 1 and 1.0 Torr for test No. 2. It is inferred that with the valve closed the measured pressure of the static system will be the same as the vapor pressure of the solid cryogen. The operating temperature of the system is inferred by the vapor pressure-temperature curve for solid hydrogen shown in Fig. 2-15. The predicted operating temperature was 9.5°K, while the temperature corresponding to the measured vapor pressure was 9.56°K and 9.53K for tests 1 and 2 respectively.

As shown in Fig. 2-13 if the system were operating in space where the pumping speed is very high, the predicted operating temperature is 8.8°K.

Although good agreement was obtained between the test data and the preliminary predictions, there were significant changes in the plumbing system when it was fabricated, so an updated prediction was made. Fig. 2-16 presents the results of this prediction, and shows the pressure drop along the various elements of the system. The measured heat rate was utilized in the predictions. The curve shows the major pressure drop in the system is due to the cooler components, the 0.47" D and the 0.62" D nipples which go from the Teflon tube through the mounting plate. The external plumbing caused a small pressure drop.

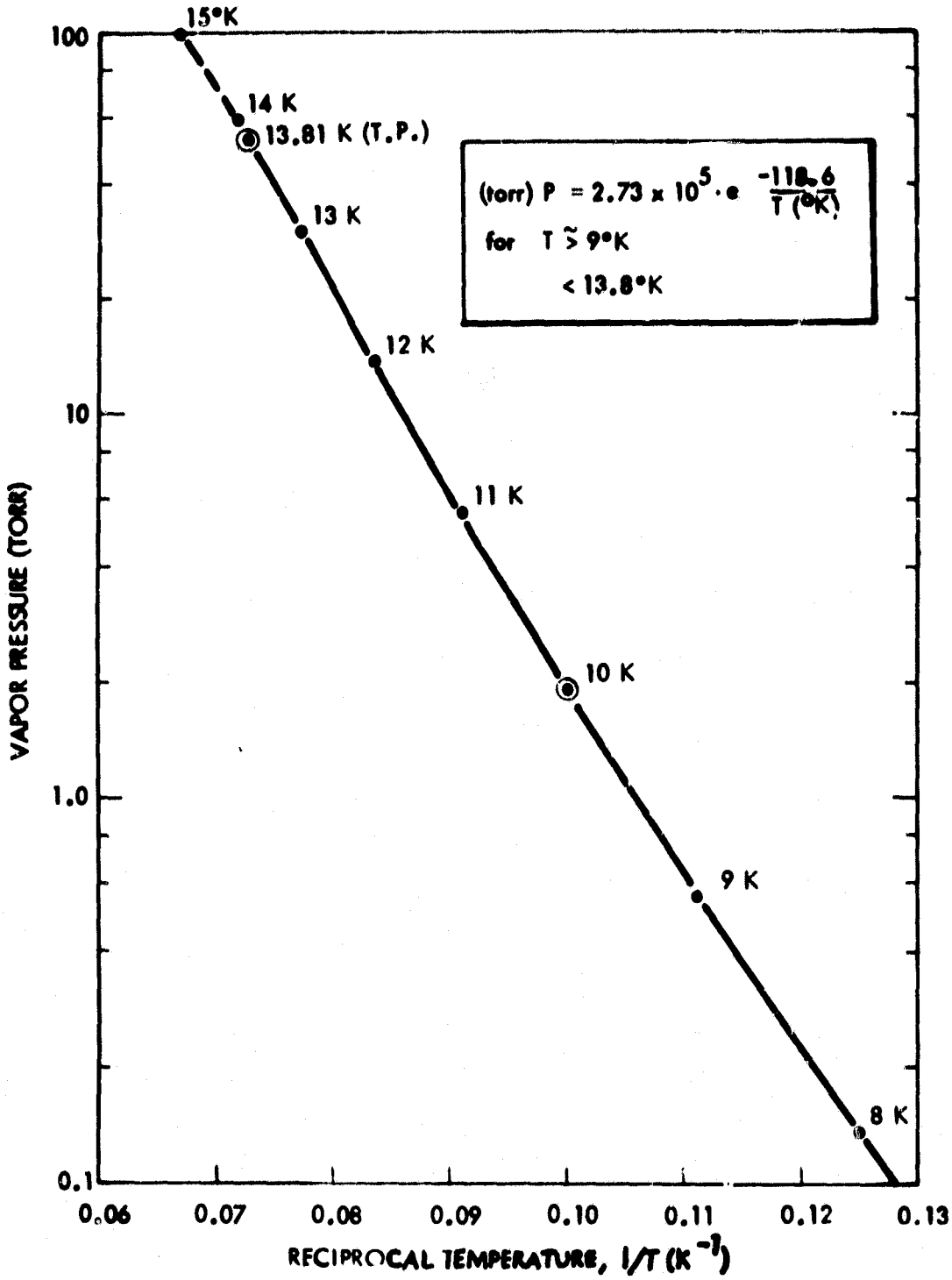

Figure 2-15. Vapor Pressure of Solid Hydrogen

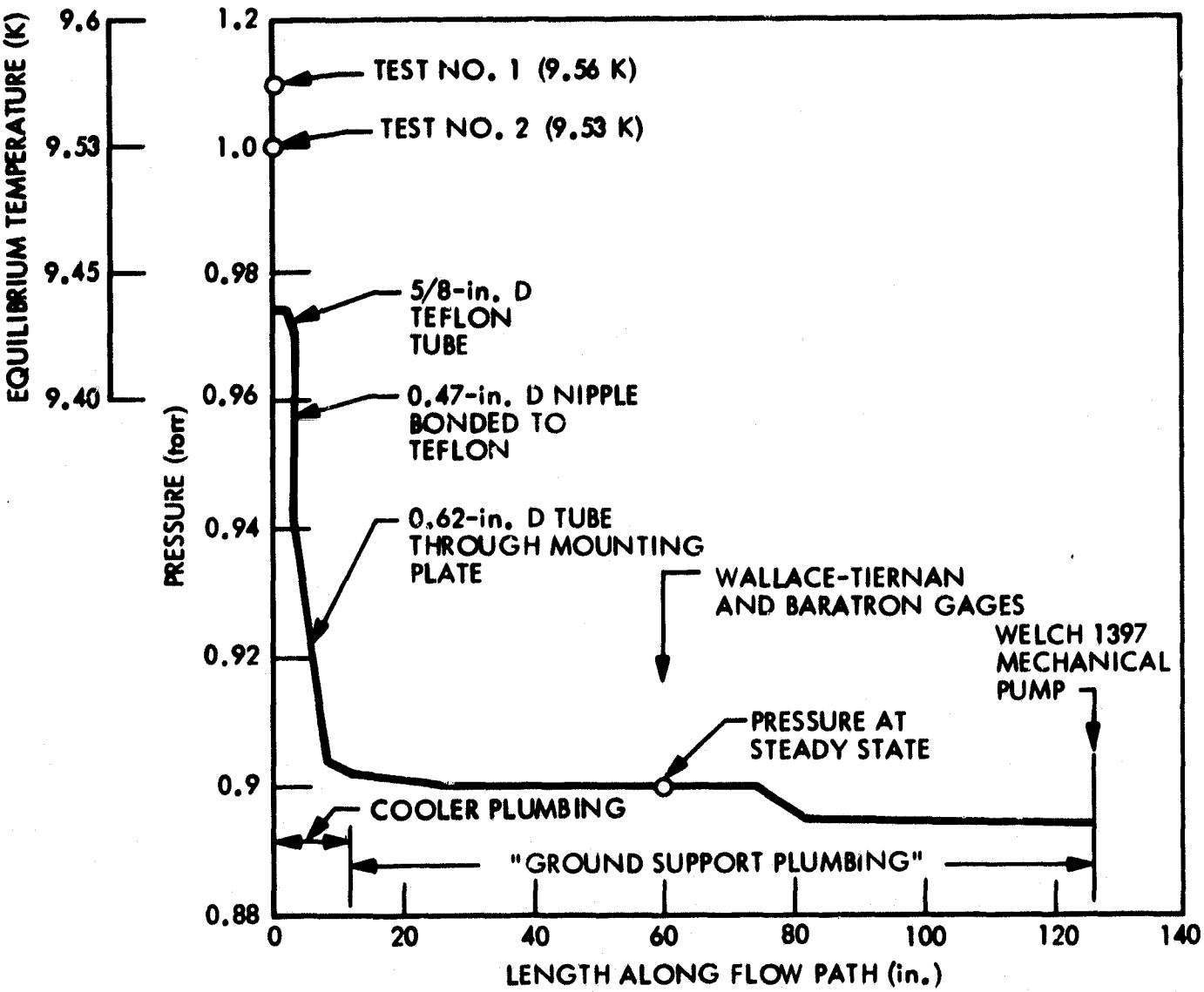

Figure 2-16. Pressure Drop Prediction for Plumbing

2.5 SYSTEM SAFETY REPORT

2.5.1 Introduction

Under Contract No. NAS 5-25792, LMSC has completed a development program to establish the feasibility of utilizing solid hydrogen in space flights for sensor and instrument cooling and to establish operating procedures which minimize the hazards normally associated with the handling of hydrogen in gaseous, liquid and solid phases.

This safety report briefly describes the cryogen system, its operation and some conclusions on the hazards associated with the system. Referenced in this report are: (1) Safety Program Plan, Appendix B; (2) System Safety Criteria, Appendix C; (3) System Hazard Analysis, Appendix D; and (4) Operational Hazard Analysis, Appendix E.

2.5.2 Safety Criteria

A System Safety Program Plan was prepared to define the program safety tasks (See Appendix B). A System Safety Requirements document was prepared to establish general system safety requirements for the design, development and testing of a solid hydrogen cooler (see Appendix C). Systems and Operational Hazard Analyses were prepared to identify existing and potential hazards which could result in death, injury, occupational illness, or damage to or loss of equipment and facilities. The standards used to evaluate the solid hydrogen cooler development are based on, but not limited to, The LMSC Safety and Industrial Hygiene Standards C-12; The National Fire Protection Association National Fire Codes, Article 500; and past experience in the handling and transporting of cryogens including liquid hydrogen.

2.5.3 Safety Summary

Safety features built into the test equipment include elimination of all sources of ignition, including complete grounding of all equipment and operating personnel in the immediate vicinity of the test, use of an explosion-proof

pump motor, electrical equipment such as switches, connectors which meet NFPA Class 1, Division II Hazardous Location requirements, automatic isolation of the cooler cryogen tank from the roughing pump in the event of power failure, vacuum gage activated alarm, a pressure relief valve vented to the facility vent in the event of overpressure, and provision for purging of the cryogen storage/vent/fill and vacuum systems.

The test facility provides explosion-proof exhaust fan and lighting, and an alarm system in the event of exhaust fan failure. A hydrogen detector system consisting of a sensor placed at the high point of the test area ceiling (outside of the ventilation hood) and a control panel with alarm conveniently located adjacent to the test area were installed.

Safety features included in the test procedure are: (1) pre-testing of the cooler by filling the cooler first with liquid nitrogen and then with liquid helium to confirm the integrity of the cooler at temperatures equal to the temperature of solid hydrogen; (2) ensuring that all equipment is grounded including equipment used for transfer of cryogens; (3) ensure that all personnel involved in the testing wear "leg stats" and wear personnel protective equipment during transfer of cryogens; and (4) ensure that the facility hydrogen detector/alarm unit is operational. Additionally, the test procedure provides detailed purging techniques to eliminate system contamination and prevent potential ice blocks in the cryogen system and the cooling system. The cooler emptying procedure provides for carefully controlled warm-up of the solid hydrogen to prevent uncontrolled release of hydrogen. Pressure, temperature and flow sensors provide continuous monitoring of the condition of the cooler during all phases of operation. Twenty-four hour surveillance of the test operation was provided during the period that hydrogen was stored in the cooler.

2.6 CONCLUSIONS

This study has confirmed the feasibility of utilizing solid hydrogen as a cooling agent for spacecraft instruments and sensors. The testing in this program was successfully conducted without incident and the experimental data

agreed well with predictions.

The measured heat rate of the system was 385 mW and was only 5% higher than the predicted value of 365 mW.

Operating temperatures of the solid hydrogen were determined by measurement of the vapor pressure and were determined to be 9.5K, compared to a predicted value of 9.5K. Calculations of the operating temperature in orbit indicate that 7.8K would be attained, due to elimination of the pressure drop in the ground support system and the better pumping capacity afforded by space.

The various operations associated with servicing the cooler consisted of filling the cooler with liquid hydrogen, freezing by liquid helium circulation, pumping to equilibrium temperature and the warm-up at the end of the test. These operations went as expected, the time to perform the fill was in the area of a few minutes, the freezing time was a few hours and the adjustment to equilibrium temperature and heat rate was several days. The quantity of liquid helium required to freeze and subcool the solid hydrogen was 8.6 lbs of liquid helium per pound of liquid hydrogen. This value is quite efficient compared with theoretical values, however, it is expected that further reductions in specific helium usage could be attained with additional testing.

If a cryogenic tank is filled 100% with liquid hydrogen and then frozen, the thermal contraction will result in an ullage space of 25% which is a substantial system penalty. Topping off of partially filled tanks should be demonstrated at some point, however, it is not anticipated that it will be difficult or require new techniques. Topping off could be performed by utilizing boil-off from a LH_2 dewar, warming the gas and then cryopumping it into the cooler to the desired capacity. Use of LH_2 boil-off is necessary to preclude heat generation from the ortho-para reaction.

One of the principal hazards associated with the solid hydrogen cooler is the possible leakage of air into the tank through valves or joints during times when the hydrogen is at low pressures (the majority of the test periods).

The resultant freezing of air in the cryogen tank can lead to a plugged vent line, which can be quite serious. To minimize or preclude this possibility it appears that a flight system should be designed from the start so that a helium purge box can cover all valve and line connection during stand-by operations. This feature would considerably reduce the possibility of this event occurring.

In the development of a flight system it would be desirable to minimize the operations with solid hydrogen, and perform as many tests as possible with a substitute cryogen, probably liquid helium. This should be considered in the logistics of a program to minimize the safety effort.

Section 3

PARA-ORTHO CATALYTIC CONVERTER ANALYSIS AND DESIGN

3.1 INTRODUCTION

Hydrogen exists in two different molecular states; the para form in which the protons have opposing spins, and the more energetic ortho form which has unidirectional proton spins. At room temperature, normal hydrogen consists of approximately 25% para and 75% ortho, while at the normal boiling point temperature of 20.4°K, the mixture is greater than 99% para. The endothermic, uncatalyzed conversion from mostly para to the equilibrium composition is an extremely slow reaction, taking hundreds of hours. However, use of appropriate catalysts can reduce the reaction time to fractions of a second. The purpose of this study is to design, build, and evaluate a catalytic converter which will use the endothermicity of the para to ortho conversion to enhance spacecraft instrument cooling with hydrogen, within the temperature range 40 to 125°K.

Two reactor configurations have been proposed, studied, and designed. Each reactor will contain approxiamtely 10 g of active catalyst and will have a pressure drop of approximately 0.25 Torr with flow rates of 0.01g H_2/sec. At this point, the radial flow design is preferred to the packed bed axial flow design for reasons of lower pressure drop for equal cross-sectional areas, and ease of packaging. To minimize pressure drops in the axial packed bed, it necessarily has to be pancake shaped; about 2-1/2" in diameter and 1/4" thick. An equivalent pressure drop radial flow reactor is only 1-1/2" in diameter while being about 2" long with a 1/4" thick radial catalyst bed.

The present test plan calls for testing of the radial flow design in a modification of the present test set-up to achieve adiabatic conditions.

Because of the unique design demands of this converter (low flow rates, temperature, pressure, and pressure drop), much of the available literature is not applicable; previous studies having concentrated on larger scale, higher

pressure, exothermic conversion of normal H_2 to equilibrium H_2 at lower temperatures. Much of the available data has been extrapolated into regimes where present knowledge is sketchy at best, but this author feels that all estimates have been overly conservative, and that during actual retesting the reactors will perform far better than expected.

3.2 APPLICATION TO FLIGHT SYSTEMS

Studies (3-1) have indicated the need to cool the optics module to below $30^{o}K$ and to provide 10W of cooling to the baffle at $100^{o}K$. This can be attained by the p-O converter operating with a hydrogen mass flow rate of slightly less than 0.01 g/sec. Figure 3-1 shows the results of a trade study comparing vapor cooling, vapor cooling with p-O conversion, and vapor cooling with mechanical refrigeration. The upper family of curves shows resultant baffle temperatures for a series of total cooling options (0W to 10W). The lower group is a similar set of curves applied to the optics box. Resultant temperatures are plotted against total gas mass flow rate (i.e., inverse lifetime). Use of the endothermic p-O conversion increases the cooling capacity and thereby extends the lifetime by about 40%

3.3 DISCUSSION OF PHENOMENA

At low temperatures, the spontaneous conversion of para-H_2 to the equilibrium composition is very slow and is attributed to magnetic intereactions between the ortho molecules. The kinetics follow a standard bimolecular rate law of $-dx/dt = Kx^2$, with an uncatalyzed rate constant $K = 0.114/hr^{3-2}$, and where x represents the concentration of a form of H_2. The equilibrium composition of H_2 versus temperature is shown in Figure 3-2.

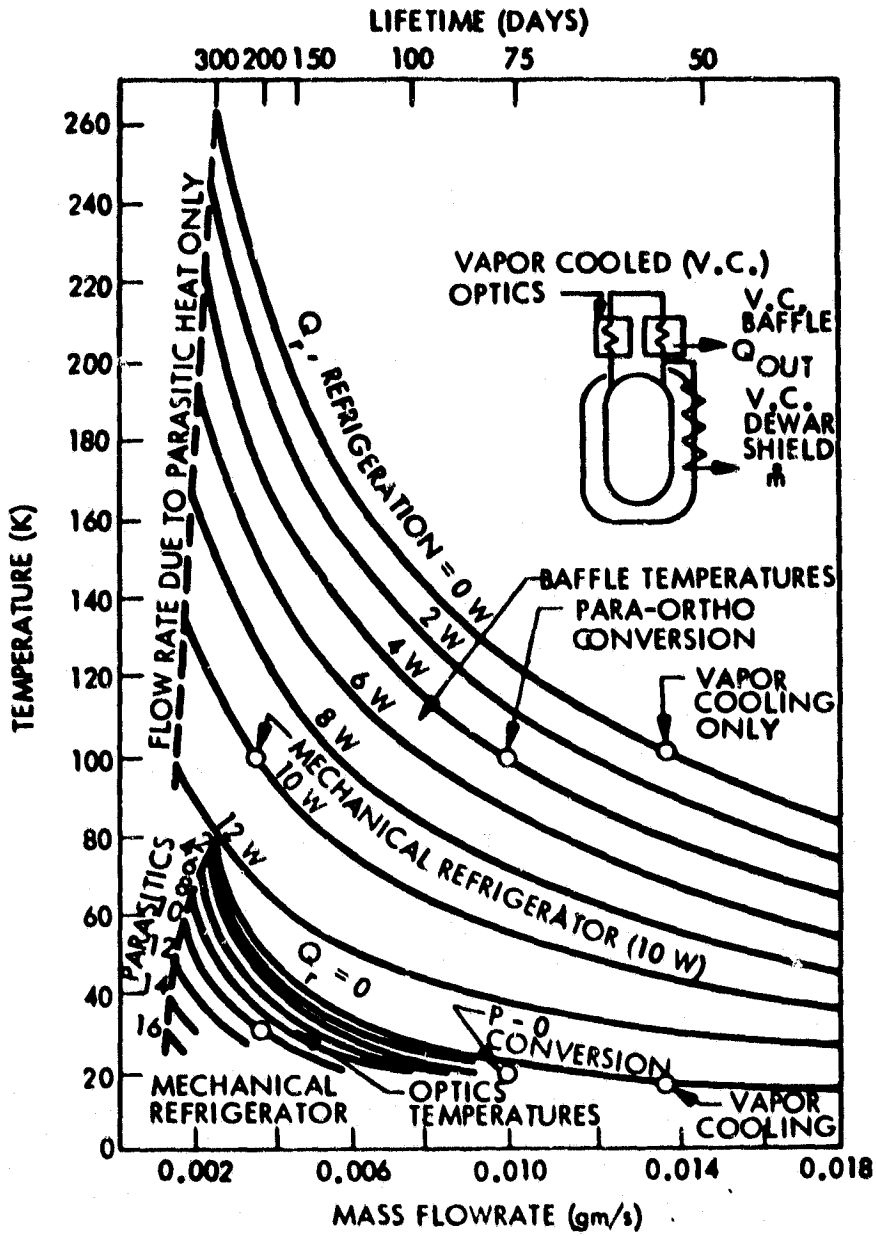

Fig. 3-1. Optics and Baffle Temperature vs Hydrogen Flow Rate

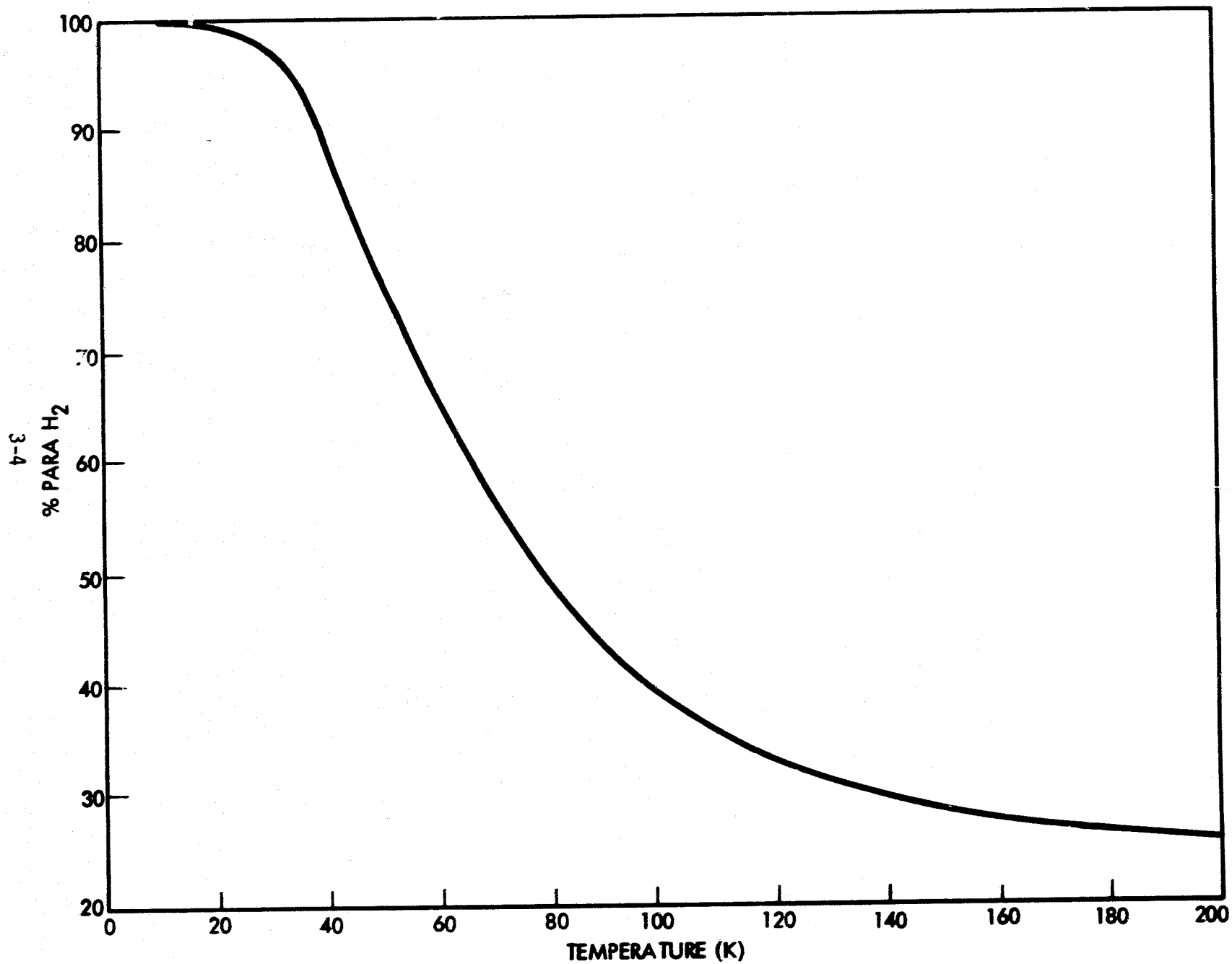

Figure 3-2. Equilibrium Composition for Hydrogen

3.4 CATALYSTS AND REACTION KINETIC PARAMETERS

An extensive literature search yielded data on activities of various catalysts; including metal films, metal hydride gels and metals supported by alumina, silica, oxides, or zeolites. In terms of a kinetic rate parameter such as Km (molecules H_2 converted per sec per mg catalyst) the most active catalysts consist of Ni, Cu, or Fe films supported by alumina or silica. Most researchers subscribe to a form of the Wigner theory of catalyst activity whereby absolute conversion rates are proportional to the square of the magnetic moment of the metal ion.

The physical mechanism of the conversion is believed to involve adsorption of the H_2 molecules on paramagnetic sites, with the overall kinetics generally following a first order Arrhenius rate law ($K_m = B_m \exp(-E/RT)$), where K_m is the catalyst specific reaction rate; B_m, the pre-exponential factor; E, the activation energy in cal/mole; and R is the specific gas constant. In addition to this mechanism, various chemical mechanisms have also been proposed. Whereas in the paramagnetic mechanism the adsorbed pH_2 molecule is magnetically switched to oH_2, the chemical mechanisms involve the splitting of the pH_2 molecule into two H atoms, each on an uncovered surface metal site of low binding energy, and then the recombination to oH_2. These are forms of the Bonhoeffer-Farkas[3-3] mechanism which has no diffusion retardation since the activity is due to the catalytic surface. The chemical mechanisms are also approximately first order reversible Arrhenius reactions. Because of the nature of the conversion mechanism, the para to ortho conversion is the kinetically reversible reaction to ortho to para conversion.

Listed below in Table 3-1 are various catalysts, experimental temperatures, pressures and relative activities found in the literature. In formulating a common basis of units for K_m, all catalysts were assumed to have an active surface area of 40 cm^2/mg, which is an approximate value obtained from the literature.

TABLE 3-1

ACTIVITIES OF VARIOUS CATALYSTS

Catalyst	T(^{o}K)	P(Torr)	$\beta(\frac{g\ catalyst}{gH_2/sec})$	$K_m(\frac{molecules}{mg/sec})$		Author
Zeolite	77-90	7	2.1×10^{6}	1.4×10^{14}	(3-4)	Rudham, 1975
Pd^{+2}/Zeolite	"	"	4.8×10^{5}	$6,2\times10^{14}$		" "
Mole Sieve	"	"	8.5×10^{4}	3.5×10^{15}	(3-5)	Brown,1970
Nd^{+3}/Mole Sieve	"	"	4.3×10^{4}	6.9×10^{15}		" "
Mn^{+2}/Zeolite	"	"	3.1×10^{4}	9.6×10^{15}	(3-4)	Rudham, 1975
Co^{+2}/Zeolite	"	"	2.5×10^{4}	1.2×10^{16}		" "
Ni^{+2}/Zeolite	"	"	2.3×10^{4}	1.3×10^{16}		" "
Cu^{+2}/Zeolite	"	"	2.0×10^{4}	1.5×10^{16}		" "
Rhenium Powder	77-368	10-180	7.5×10^{3}	4.0×10^{16}	(3-6)	Kubicka, 1971
Dy_2O_3	-	7.6	1.0×10^{3}	3.0×10^{17}	(3-7)	Eley, 1974
Ni; NiH_2 Films	170-195	2	1.0×10^{3}	3.0×10^{17}	(3-8)	Frankiewicz, 1975
Nd_2O_3	-	7.6	6.4×10^{2}	4.7×10^{17}	(3-7)	Eley, 1974
Fe	90	1.2	5.7×10^{2}	5.2×10^{17}	(3-9)	Eley, 1963
Fe	273	1.2	5.2×10^{2}	5.7×10^{1}		" "
Ni	"	1.2	4.5×10^{2}	6.7×10^{17}		" "
Co	"	1.2	4.0×10^{2}	7.4×10^{17}		" "
Fe_2O_3 gel			8.8×10^{1}	3.4×10^{18}	(3-10)	Weitzel
$NiO{\cdot}2.5\ SiO_2$ gel			3.6×10^{1}	8.4×10^{18}	(3-11)	Singleton, 1967

On the next pages are two tables whose data could not be converted to the common K_m basis. They give an indication of the relatively high activities of the Ni/Al_2O_3 catalysts, however, note that the order of the most active catalysts (Ni/Al_2O_3 and hydrous ferric oxide gel) vary according to each author and method of preparation.

TABLE 3-2[3-12] ACTIVITIES OF SOME OTHER CATALYSTS

	Catalyst Sample	T	Density (g/cm^3)	Wt (g)	Pressure (atm)	Act. Ener. (E) Kcal/mole	K	Relative Activity
	19% Cr_2O_3/Al_2O_3	77°K	1.34	9.30	28.2 7.8 4.4	0.99 0.99 0.99	0.099×10^{-4} 0.076×10^{-4} 0.060×10^{-4}	1.0
	0.5% CuO/Al_2O_3		1.26	3.86	28.2 7.8	0.97 0.98	0.33×10^{-4} 0.27×10^{-4}	3.3
	0.5% NiO/Al_2O_3		1.43	3.66	28.2 7.8	0.95 0.96	0.51×10^{-4} 0.34×10^{-4}	5.2
	0.5% Cu/Al_2O_3		1.26	3.86	28.2 7.8	- -	0 0	0
	0.5% $Ni(A)/Al_2O_3$		1.43	3.66	28.2 7.8 4.4	0.77 0.81 0.85	3.0×10^{-4} 2.2×10^{-4} 1.7×10^{-4}	30
	Ferric Oxide Gel (Weitzel)							4.0
Most Active on a Wt.basis	0.5% $Ni(B)/Al_2O_3$		1.33	3.21	28.4 4.4	0.70 0.81	5.2×10^{-4} 2.7×10^{-4}	53
	0.5% Mn_2O_2/Al_2O_3		1.28	3.38	28.2 7.8	0.94 0.95	0.76×10^{-4} 0.63×10^{-4}	7.7
	0.5% Tb_2O_3/Al_2O_3		1.69	4.70	28.2 7.8	0.93 0.94	0.41×10^{-4} 0.32×10^{-4}	4.1
	0.5% Pd/Al_2O_3		1.41	4.11	28.2 7.8	- -	0 0	0
	5.0% $Ni(I)Al_2O_3$		1.84	3.84	28.2 7.8	0.85 0.86	0.84×10^{-4} 0.69×10^{-4}	8.5
	5.0% $Ni(X)\ Al_2O_3$		1.91	2.55	28.2 7.8	0.42 0.45	8.9×10^{-4} 5.7×10^{-4}	90
	0.5% TbO_2/ZrO_2		3.63	6.58	28.2 7.8 4.4	0.96 0.97 0.98	0.20×10^{-4} 0.17×10^{-4} 0.11×10^{-4}	2.0

TABLE 3-3 RELATIVE CATALYST ACTIVITIES

CONVERSION OF 25% PARA TO 90% PARA AT 20°K, 15 PSIG

CATALYST	SPACE VELOCITY (STP/min)	RELATIVE SPACE VELOCITY (Cr_2O_3 = 1)
Gadolinium oxide, unsupported WORST	10	0.2
Crude Ceria oxide, unsupported	20	0.4
Neodymium oxide, unsupported	20	0.4
$FeCl_3$ on silica gel	20	0.4
2% Peremag Fe_3O_4 on porous glass	20	0.4
15% Peremag Fe_3O_4 on 'Fiberex'	24	0.5
Ferric ammonium sulfate, unsupported	30	0.6
Magnetite, Fe_3O_4, unsupported	40	0.8
20% Cr_2O_3 on alumina (Harshaw)	50	1.0
18 % Peremag Fe_3O_4 and 9.3% Cr_2O_3 on alumina	50	1.0
5.3% Ni and 0.24% Thoria on alumina	60	1.2
18% MnO_2 on silica gel	80	1.6
0.5% Ni on alumina	100	2.0
Hydrous manganese dioxide, unsupported	190	3.8
Hydrous Ferric oxide, unsupported BEST	330	6.6

Table 3-3 shows relative catalyst activities for conversion of a 25% para stream to 90% para at 20°K and 15 psig pressure. Activities are presented in terms of relative space velocities; the hydrogen flow (ℓSTP/min) which will be converted to 90% para, compared to the 50 ℓSTP/min conversion achieved with a 20% Cr_2O_3 on alumina reference catalyst whose relative space velocity is set equal to unity. The greater the relative space velocity, the greater the catalyst activity under these conditions.

Two methods were used to determine β, the amount of catalyst required to convert a hydrogen mass flow (g catalyst/gH_2/sec) to the equilibrium composition. The data in Tables 3-1 and 3-2, km (the reaction rate constant) for high activity catalysts under the conditions of this study, ranges in value from 3.0×10^{17} to 8.4×10^{18} molecules H_2/sec/mg catalyst. A flow rate of .01g H_2/sec represents 3×10^{21} molecules H_2/sec/gm, therefore a range of appropriate β would be 36 to 1000.* The second method utilizes β values from published experimental data. The data from Tables 3-1 and 3-2 are shown on Fig. 3-3, a plot of β versus pressure. Table 3-4 data representing very high (>95%) percentage conversions to equilibrium compositions for the APACHI-1 catalyst (a high surface area Ni on a Silicate support), and Table 3-1 data for very high activity catalysts are connected to fall within a range of acceptable β values. A β of about 370 at the design pressure of 2 torr appears

* $$\frac{3 \times 10^{21}}{Km} = \frac{\text{mg catalyst}}{.01 g H_2/\text{sec}} = \beta \times 1000$$

TABLE 3-4. APACHI-1 CATALYST ACTIVITY

Point	Tin(^{o}K)	P(psia)	M(g/sec)	Dp(mesh)	$\beta(\frac{g\ catalyst}{gH_2/sec})$	% equilibrium conversion
1	86.7	51	.668	16-25	104.	94.3
2	97.8	54	.643	30-40	61.8	100
3	76.7	54	.655	30-40	80.8	98.5
4	110	54	.630	30-40	84.	99.9
5	97.2	54	.630	30-40	82.4	99.8
6	86.7	54	.643	30-40	82.4	96.5
7	86.7	54	.428	30-40	124.	98.8
8	70.6	54	.643	30-40	61.8	99.2
9	132.8	53	.668	16-25	104.	96.0
10	132.8	51	.435	16-25	160.	99.7
11a	119.4	54	.605	30-40	110.	99.7
11b	119.4	54	.605	30-40	87.7	99.0
12	90.	54	.643	30-40	82.4	100.
13	67.2	54	.655	30-40	80.8	100.
14	56.1	54	.655	30-40	80.8	99.5
15	147.8	53	.504	50-80	117.	98.3
16	110.	53	.580	50-80	81.6	99.6
17a	88.9	53	.605	50-80	78.	100.
17b	88.9	53	.605	50-80	74.9	100.
18	79.4	53	.605	50-80	78.	100.
19	67.2	53	.630	50-80	74.9	100.
20	56.7	53	.643	50-80	73.5	100.
21	133.9	55	.643	16-25	102.	99.5
22	88.9	54	.491	80-140	83.9	93.9
23	122.8	55	.416	80-140	99.	64.7
24	111.1	54	.454	80-140	90.8	81.5
25	100.	54	.491	80-140	83.9	90.
26	66.7	54	.567	80-140	52.5	96.4
27	56.1	54	.580	80-140	51.3	96.4
28	147.2	54	.340	80-140	121.	26.7

Table 3-4 continued

Point	Tin(^{o}K)	P(psia)	M(g/sec)	Dp(mesh)	$\beta(\frac{g\ catalyst}{gH_2/sec})$	% equilibrium conversion
29	144.4	54	.340	80-140	121.	26.7
30	141.7	54	.353	80-140	117.	32.1
31	138.9	54	.325	80-140	113.	36.6
32	76.1	54	.567	80-140	53.7	99.3
33	100.	1005	.630	50-80	23.6	92.7
34	99.4	1040	1.273	50-80	11.8	68.9
35	143.9	1525	.630	50-80	23.6	77.7
36	121.7	1534	.617	50-80	24.2	87.8
37	100.	1516	.617	50-80	24.2	94.8
38	78.9	1510	.617	50-80	24.2	96.0
39	99.4	1519	1.273	50-80	11.8	70.5
40	100.6	1016	.592	50-80	25.1	91.5
41	100.	502	.592	50-80	25.1	92.5
42	122.2	997	.617	50-80	24.2	83.5
43	111.1	1525	.630	50-80	23.6	89.0
44	88.9	1514	.630	50-80	23.6	94.8
45	77.8	1010	.592	50-80	25.1	90.8
46	144.4	1520	.617	30-40	26.8	89.4
47	122.2	1528	.630	30-40	26.2	93.0
48	100.	1517	.617	30-40	26.8	96.0
49	100.	1510	1.285	30-40	12.9	75.0
50	122.2	1006	.617	30-40	26.8	92.5
51	99.4	1028	.617	30-40	26.8	94.5
52	100.	1021	1.273	30-40	13.0	75.0
53	77.2	1022	.617	30-40	26.8	97.6
54	100.	512	.617	30-40	26.8	96.1
55	78.3	1499	.617	30-40	26.8	95.8
56	98.9	1510	.617	16-25	27.5	94.0

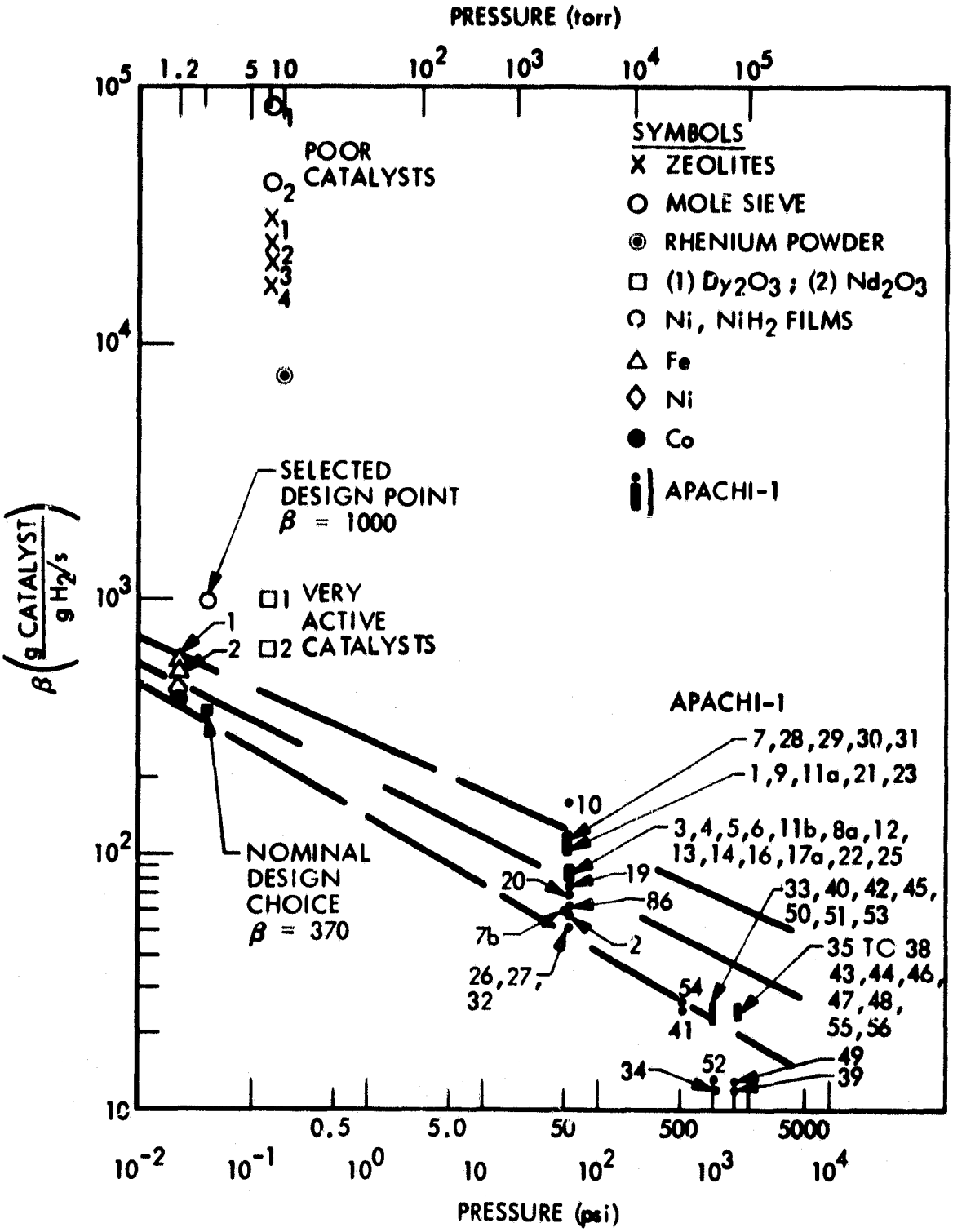

Figure 3-3. Catalyst Activity Studies; β vs. Pressure for a Variety of Catalysts, Experimental Data

to fall on the line of very high activity catalysts. The chosen design point of β equal to 1000 at the design pressure falls slightly above this range, being more representative of catalysts of moderate activities (Ni films). Thus it is felt that this is a very conservative value for this study, and actual operations should yield full conversions at lower β values.

Note that the decrease in β and increase in percentage conversion is minimal as mesh number increases. The temperature, pressure, and flow rate dependencies are much more important, with β generally increasing for decreases in all three variables. Therefore, a particle mesh size of 15, at an operating pressure of about 2 torr and temperature of $100^{o}K$, is slightly less reactive than smaller catalyst particles (mesh 20-50), but this is more than offset by the decreased flow pressure drop around larger particles.

According to industry experts (Air Products and Chemicals, Inc) the most active catalyst for the conditions of this study would be their APACHI-1, and it has been reported that this catalyst has an activity eleven times greater on a weight basis than the standard ferric-oxide gel, or an approximate K_m of 3.7×10^{19} molecules H_2/mg catalyst/sec.[3-10] Accordingly, for this study, the APACHI-1 catalyst has been selected and a conservative K_m of 3×10^{17} was used in the calculations.

3-5 PROCESS OPTIONS

Figures 3-4, 3-5, 3-6 are enthalpy-temperature plots representing the overall thermodynamics of the catalytic conversion system. Figure 3-4 shows lines of 100% para and equilibrium compositions. Figures 3-5 and 3-6 show an equilibrium composition line and % para lines from 0 to 100% in increments of 10%. This allows more precise determination of state point compositions.

Three operating process alternatives are of interest: an adiabatic catalytic converter, an isothermal reactor, and no reactor. All options use heat exchange from the baffle to warm the hydrogen gas from 30°K (optics temperature) to 100°K (baffle temperature); (points (1) to (2)) on the process diagrams; figs. 3-4, 3-5, 3-6). At this point, because of the slow rates of equilibration, the gas stream is still almost completely in the form of para-hydrogen. In the adiabatic reactor, the catalyst causes the gas to quickly reach nearly 100% of its equilibrium composition along a line of constant enthalpy. Since the para to ortho conversion is an endothermic process, energy is removed from the gas, causing the temperature to drop to about 79°K. The equilibrium composition at this point ((2a) on the process diagrams) is 49% para. Because of the very slow uncatalyzed reaction rates in the exit line, the gas is warmed by the baffle along a line of constant composition (49% para) to a final temperature of 100°K (Point (4) on the process diagrams), a process which contributes an additional 314 J/g cooling capacity to the uncatalyzed case(1107 J/g vs 793, J/g, respectively). Ten watts of cooling may therefore be attained by the adiabatic reactor with a hydrogen mass flow rate of 0.00903 g/sec. With a flow rate equal to 0.01 g/sec, 10W of cooling may be extracted from a 112.5°K baffle, or 11.1 W from a 100°K baffle.

The isothermal reactor utilizes heat from the baffle to maintain a constant gas temperature during a continuous conversion to the equilibrium composition of 38.6% para at 100°K (point (3) on the process diagrams). There is no further heat exchange in the exit line. The enthalpy difference between the final two states is 368.4 J/g, yielding a total cooling of 1181.4 J/g, which is the

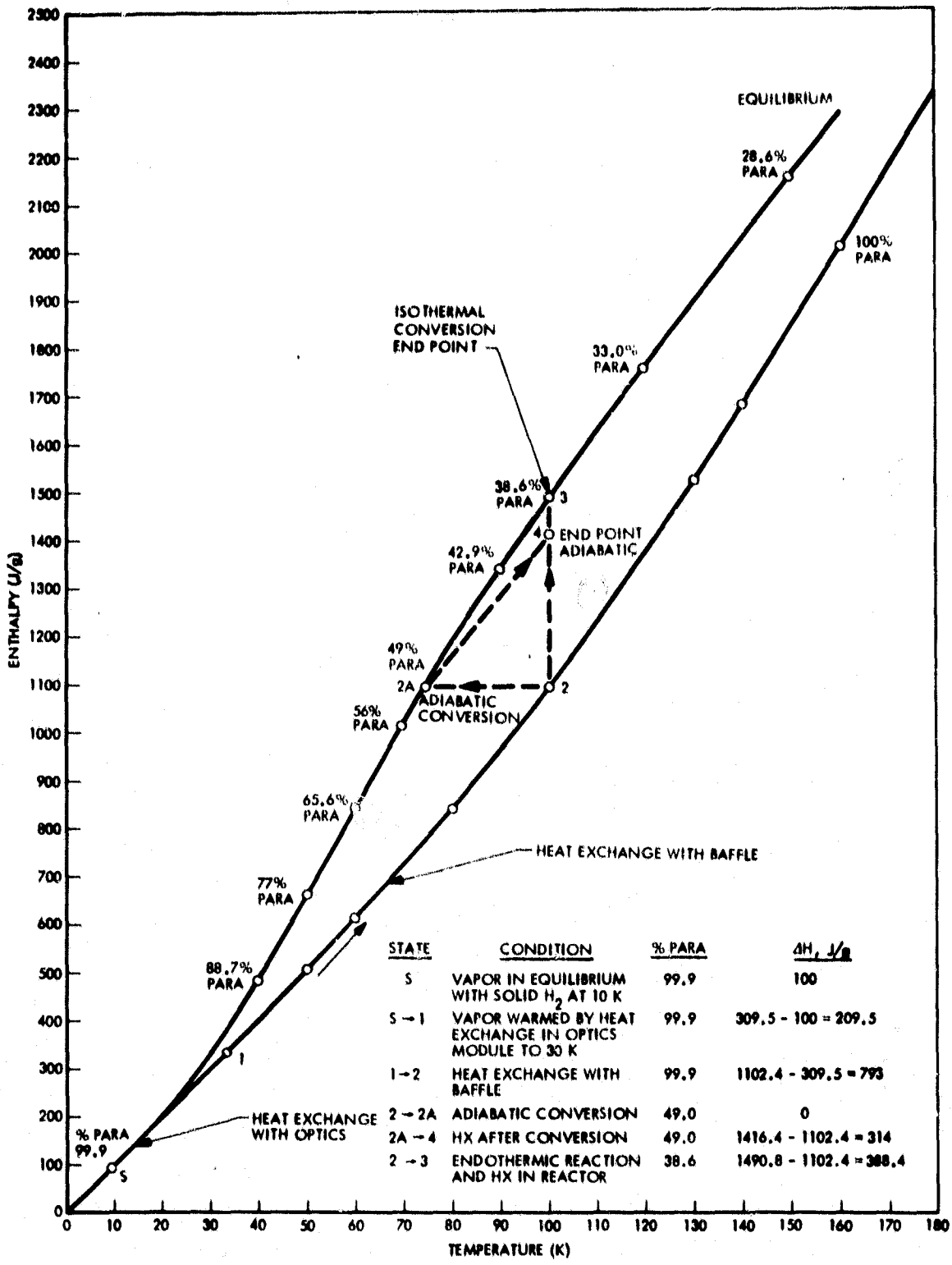

Figure 3-4. Overall System Process Diagram

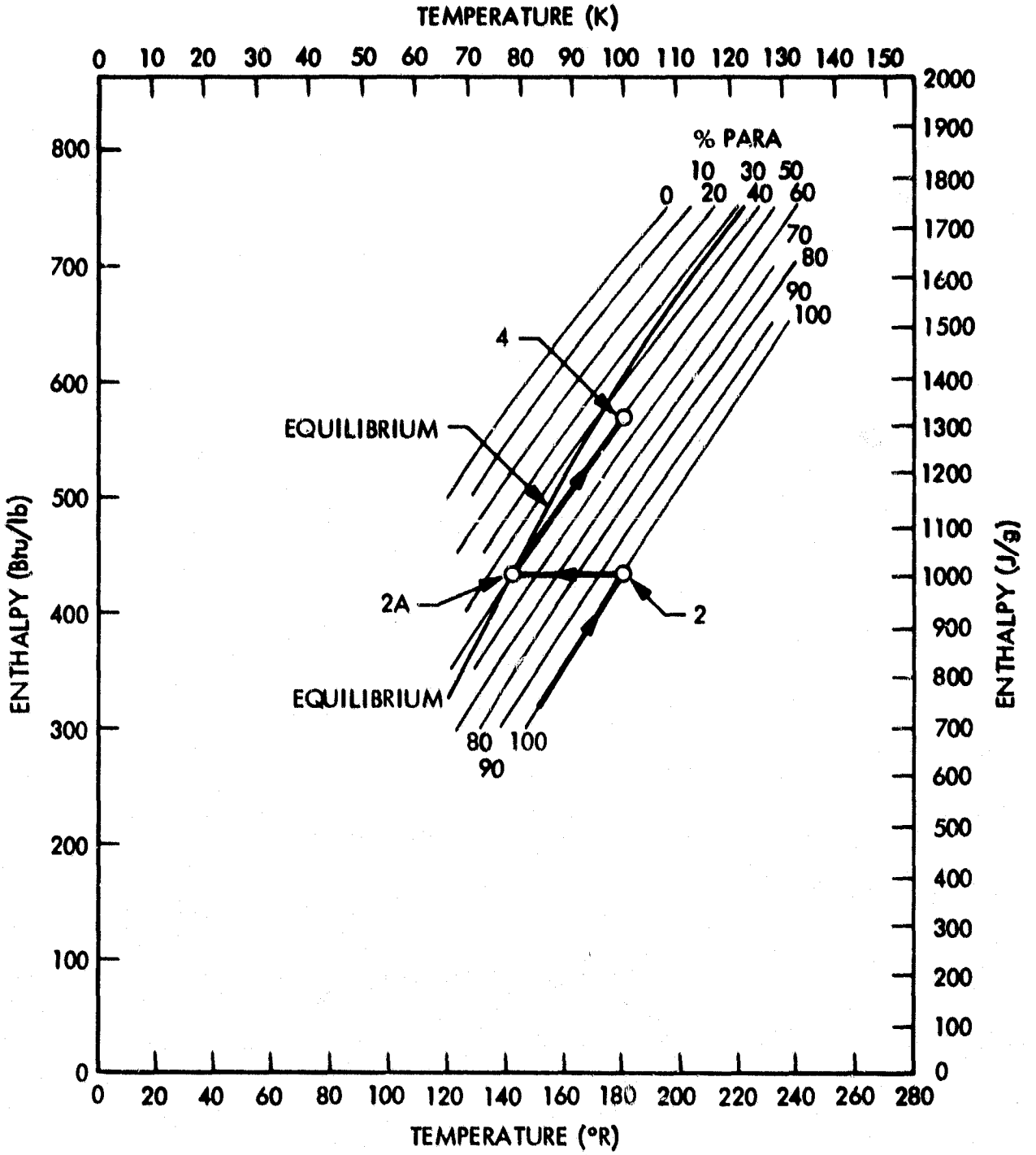

Figure 3-5 Adiabatic Process Diagram

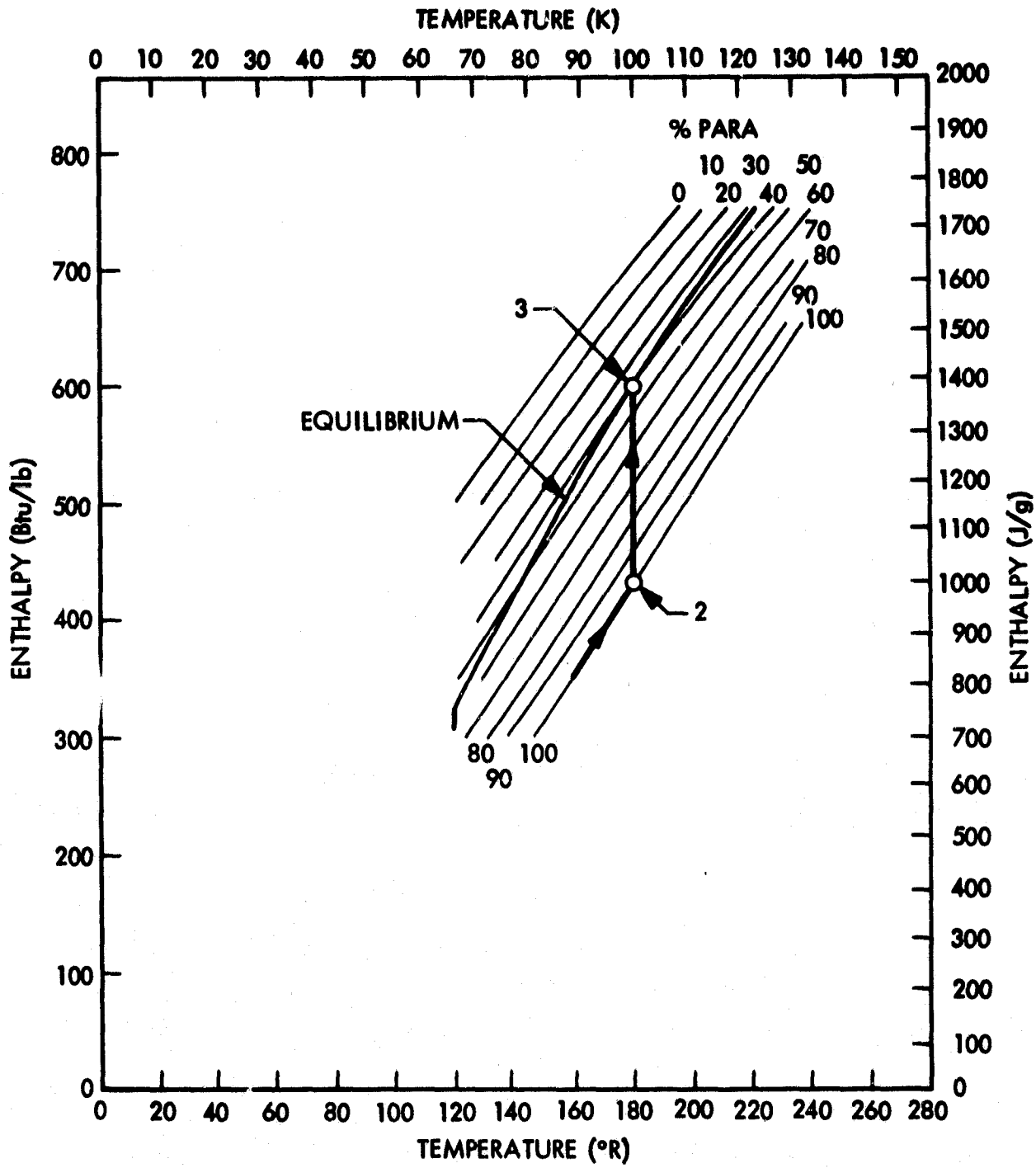

Figure 3-6. Isothermal Process Diagram

greatest cooling capacity of the options. For comparison, the adiabatic reactor is only 93.7% as effective, and the non-reactor case has 67.1% of the cooling capability.

The test reactor will be designed for adiabatic operation, due to the difficulties inherent in insuring adequate heat transfer in the small catalyst space, as is required by the isothermal condition. However, because of heat leaks from the test apparatus to the reactor, actual operation will be between the adiabatic and isothermal conditions.

Note that the absolute enthalpies on the two process diagrams differ. This is due to different sources using different reference datum points. However, enthalpy differences are consistent.

The analysis is summarized in the following material and in Table 3-5.

TABLE 3-5

State Point Enthalpies

State/Process	H(J/g)	ΔH(J/g)	Description
1	309.5		30^{o}K gas from optics
2	1102.4		100^{o}K gas from baffle
1→ 2		792.9	Cooling of baffle without catalytic converter
	1102.4		78.9^{o}K, 49% para
2→ 2A		0	adiabatic conversion
3	1490.8		100^{o}K, 38.6% para
2→ 3		388.4	Isothermal conversion
4	1416.4		100^{o}K, 49% para
2A→ 4		314.	Heating of state 2A gas to final temperature
Adiabatic Converter		1107	1→ 2 → 2A → 4
Isothermal Converter		1181.4	1→ 2 →3

TOTAL PROCESS REPRESENTATIONS

- o 3 alternative modes of operation
- o gas from optics at $30^{o}K$
- o baffle at $100^{o}K$
- o H_2 mass flow rate $\dot{M}$ = .01 g/sec
- o vapor pressure 1.9 torr

1) No converter

$\Delta h_{1 \rightarrow 2}$ (1102.4 - 309.5 J/g) = 793. J/g

cooling capacity at $\dot{m}$ = 7.9W

2) Adiabatic catalytic reactor

$\Delta h_{1 \rightarrow 2}$ = 793.0

$\Delta h_{2 \rightarrow 2A}$ = 0 J/g

$\Delta h_{2A \rightarrow 4}$ = 314. J/g

Δh Total = 1107 J/g

cooling capacity at $\dot{m}$ = 11.1W

$\dot{m}$ needed for 10W cooling capacity = .00903 g/sec

Baffle temperature which may be cooled with $\dot{m}$ = .01g/sec

and 10W heat extraction, = $112.5^{o}K$

3) Isothermal catalytic reactor

$\Delta h_{1 \rightarrow 2} = 793.0$ J/g

$\Delta h_{2 \rightarrow 3} = 388.4$ J/g

$\Delta h_{total} = 1181.4$ J/g

cooling capacity at $\dot{m} = .01$ g/s = 11.8W

$\dot{m}$ needed for 10W cooling capacity = .008465 g/sec

Effective Comparison

1) no reactor = 793.0 J/g = 67.1%

2) adiabatic = 1107.0 J/g = 93.7%

3) isothermal = 1181.4 J/g =100 %

-- Actual reactor will be between adiabatic and isothermal conditions.

3.6 CONVERTER DESIGN STUDIES

After a thorough review of pertinent catalysts for the para-to-ortho conversion, the highly active APACHI-1 catalyst, a nickel on a silica support, available from the Houdry Division of Air Products and Chemicals, Inc., was the one selected for the design and experimental tests. As previously mentioned, an overly conservative value of β was chosen to be 1000g catalyst per g H_2/sec flow rate. This amount of catalyst should provide enough gas residence time for the complete conversion to the equilibrium composition.

Pressure drop through the catalyst bed was calculated using the Ergun relationship for pressure drop through packed beds with negligible static head and for particles of similar size and shape. The relationship may be expressed as:

$$\frac{\Delta P}{L} = \frac{150(1-\epsilon)^2}{\epsilon^3} \frac{\mu U_m}{D_p^2 g_c} + \frac{1.75(1-\epsilon) G U_m}{\epsilon^3 D_p g_c}$$

where

G = ρU = mass flowrate of fluid in tube; lb_m/ft^2 sec

U_m = superficial fluid velocity at average pressure; ft/sec

D_p = particle diameter, ft

ϵ = fractional void volume in bed

μ = fluid viscosity at average temperature and pressure; lb_m/ft sec

$\frac{\Delta P}{L}$ = pressure drop per unit length; $lb_f/ft^2/ft$

U = superficial fluid velocity based on empty column cross section; ft/sec

Since $G = \rho U = \dot{m}/A$, $g_c = 32.2$ ft lb_m/lb_f sec^2, and ϵ was assumed equal to 0.45, (a value obtained from the literature) the Ergun equation may be simplified to:

$$\frac{\Delta P}{L} = \left[\frac{82.5\mu}{D_p} + 1.75G\right] \frac{0.1874G}{D_p\rho}$$

The first term is the viscous contribution while the second part is the energy term. The pressure drop is dependent upon the size and shape of the catalyst particles and not upon the material. Therefore, this equation is valid for any catalyst.

Two design options were considered: a packed bed and a radial flow reactor. Because of the low pressure drop limitations, the packed bed must be thin and have a large cross-sectional area, much like a pancake. In the radial flow reactor, gas enters through a central tube and flows radially outward through the toroidal catalyst bed and into the outer annulus, whence it flows axially out of the reactor section. For an equivalent reactor diameter and catalyst weight, the radial flow reactor has much less pressure drop than the packed bed. The only advantage inherent in the latter lies in its relative simplicity. To achieve pressure drops about equal to those in the radial flow reactor, the packed bed must have a bed diameter of 2.5 inches. This leads to a very thin bed (0.28") under the constraint of a fixed $\beta = 1000$.

Figures 3-7 and 3-8 show reactor pressure drop as a function of particle mesh size, reactor length, and radial size. Each line represents a combination of particle and radial size; inner tube diameter and annulus width for the radial flow reactor and bed diameter for the packed bed. The abscissa for the packed bed reactor is reactor length. Fixing an appropriate length determines β for each specific bed diameter. For the radial flow reactor, the abscissa is the catalyst thickness, which together with the other two radial dimensions, and the catalyst packing density, determines β. These graphs suggest the following dimensions for each type of reactor.

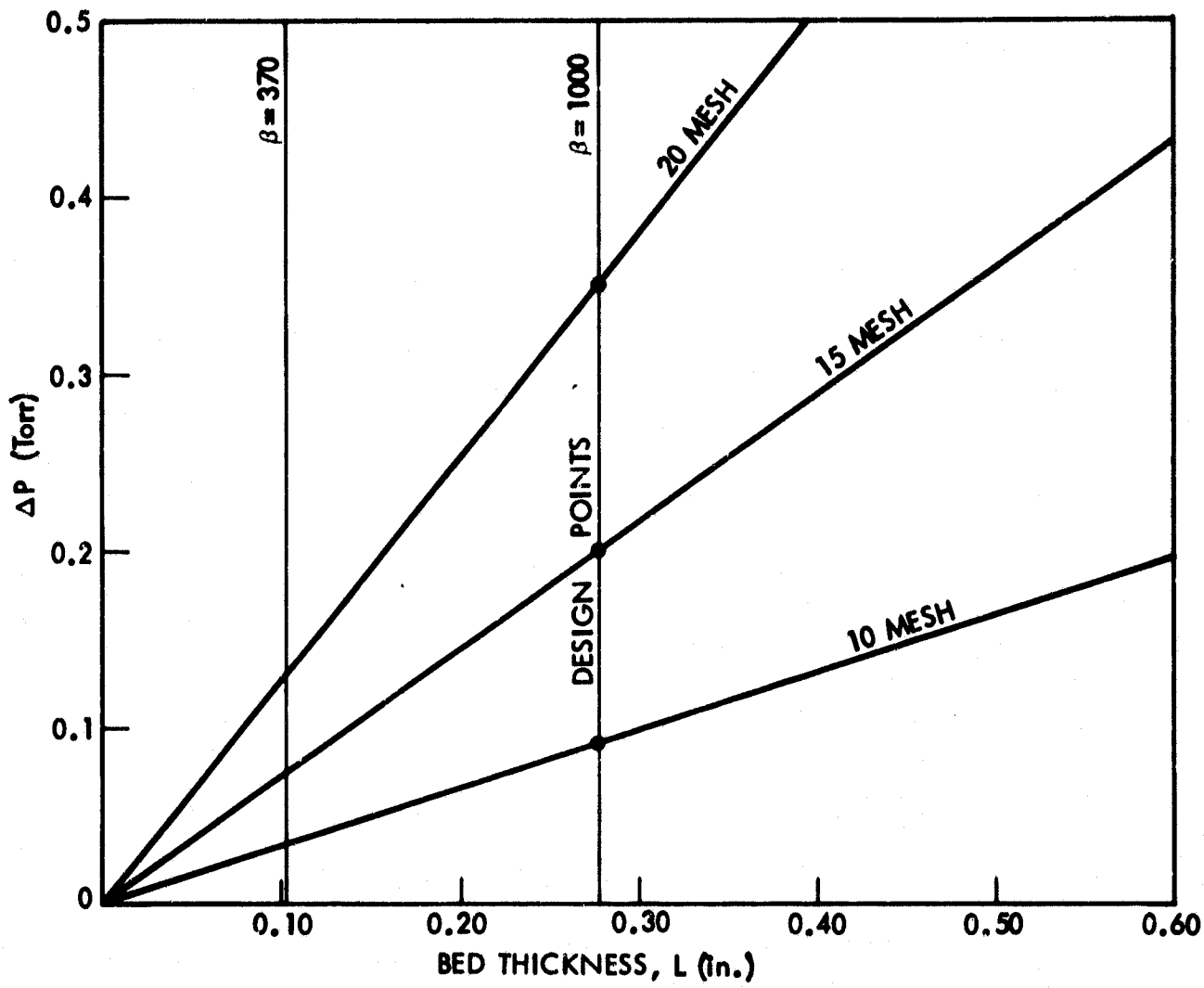

Figure 3-7. Packed Bed Reactor Pressure Drop

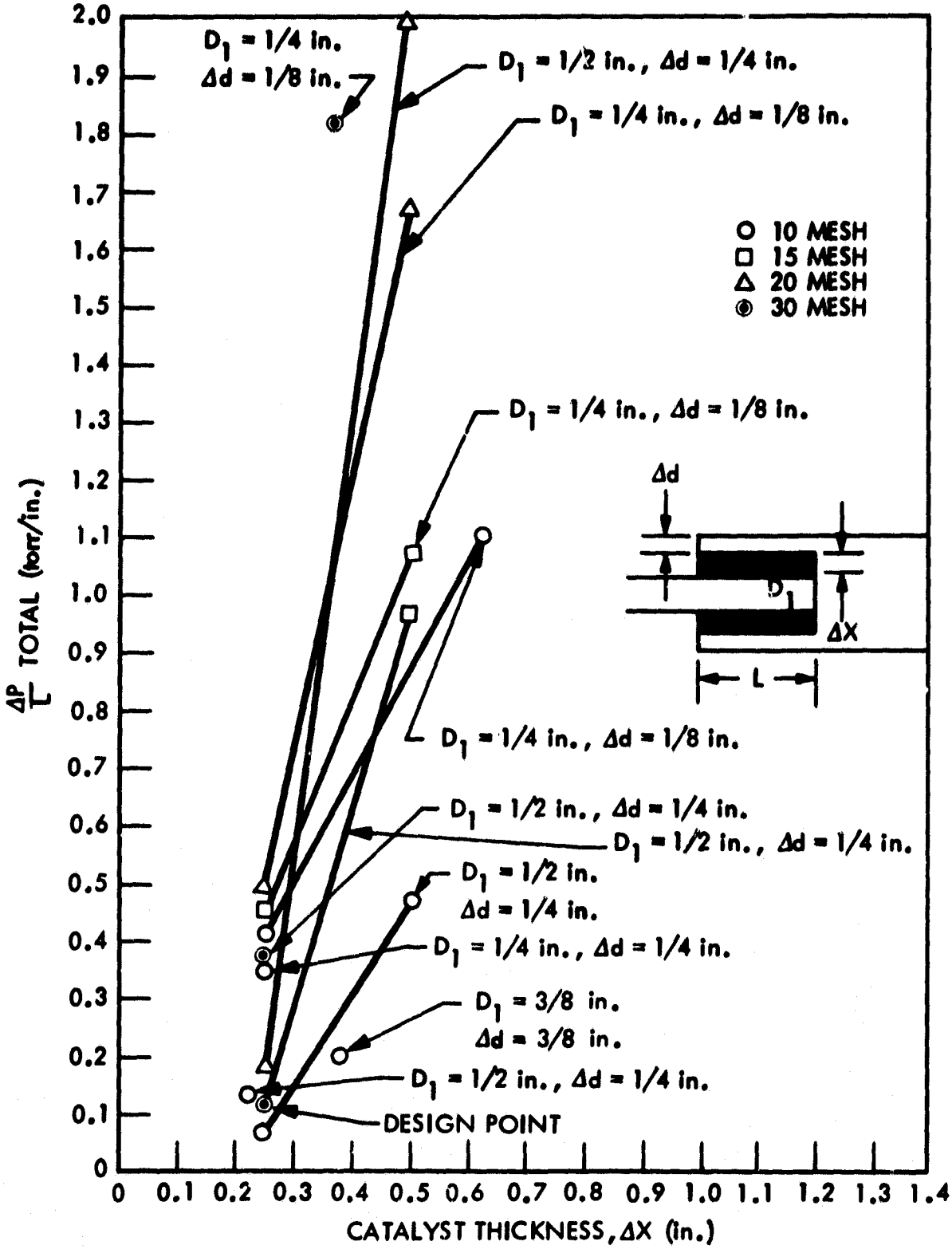

Figure 3-8. Radial Flow Reactor Pressure Drop

The radial flow reactor has an inlet tube diameter of 0.5 inch, a catalyst bed radial thickness of 0.25 inch and an axial length of 2.073 inches, and an outer annulus of 0.25 inches. The total inside diameter is 1.5 inch, with a packed catalyst weight of 10.0 grams. Pressure drops through the reactor for 10, 15 and 20 mesh particles are predicted to be 0.13, 0.23, and 0.37 torr, respectively, for a mass flow rate of 0.01 g H_2/sec, an inlet temperature of 100°K, and an inlet pressure of 2 Torr, which is the vapor pressure of gas over solid hydrogen at about 10°K. Assuming an estimated pressure drop of 2 torr through the entire system plumbing, a reactor inlet pressure of 2 torr will use all the available pressure of the gas.

For a β equal to 1000, bed thicknesses for packed bed reactors are shown in Table 3-6 A representative value, obtained from the literature[3-14], of 0.45 g/cc for the catalyst packing density was used in the calculations. This value was assumed to be independent of mesh size.

Table 3-6

Packed Bed Reactor Thickness and Pressure Drop

I.D.(in)	L (thickness) (in)	Mesh#	ΔP (torr)
1.5	.767	10	0.73
1.5	.767	15	1.59
1.5	.767	20	2.78
2.0	.432	10	0.22
2.0	.432	15	0.49
2.0	.432	20	0.86
2.5	.276	10	0.09
2.5	.276	15	0.20
2.5	.276	20	0.35

Because the pressure drops for the 2.5" I.D. packed bed reactor are similar to those of the radial flow reactor, it was chosen as a second design.

Design sketches are shown in Figures 3-9 and 3-10.

Contamination Problems

The catalyst will be screened to assure particle size control and fine screen will be utilized for catalyst containment, thereby minimizing system component contamination. The catalyst itself may be poisoned, and suffer gradual degradation in its activity, as a result of adsorbing contaminants such as water vapor, CO_2, and O_2. Careful operational procedures when activating the catalyst, building the reactor, and installing the reactor assembly into the system will minimize this problem. Should these procedures prove inadequate or procedural errors occur, a method for catalyst re-activation via heating might be probed, providing it is feasible within the test plan and compatible with the flight system.

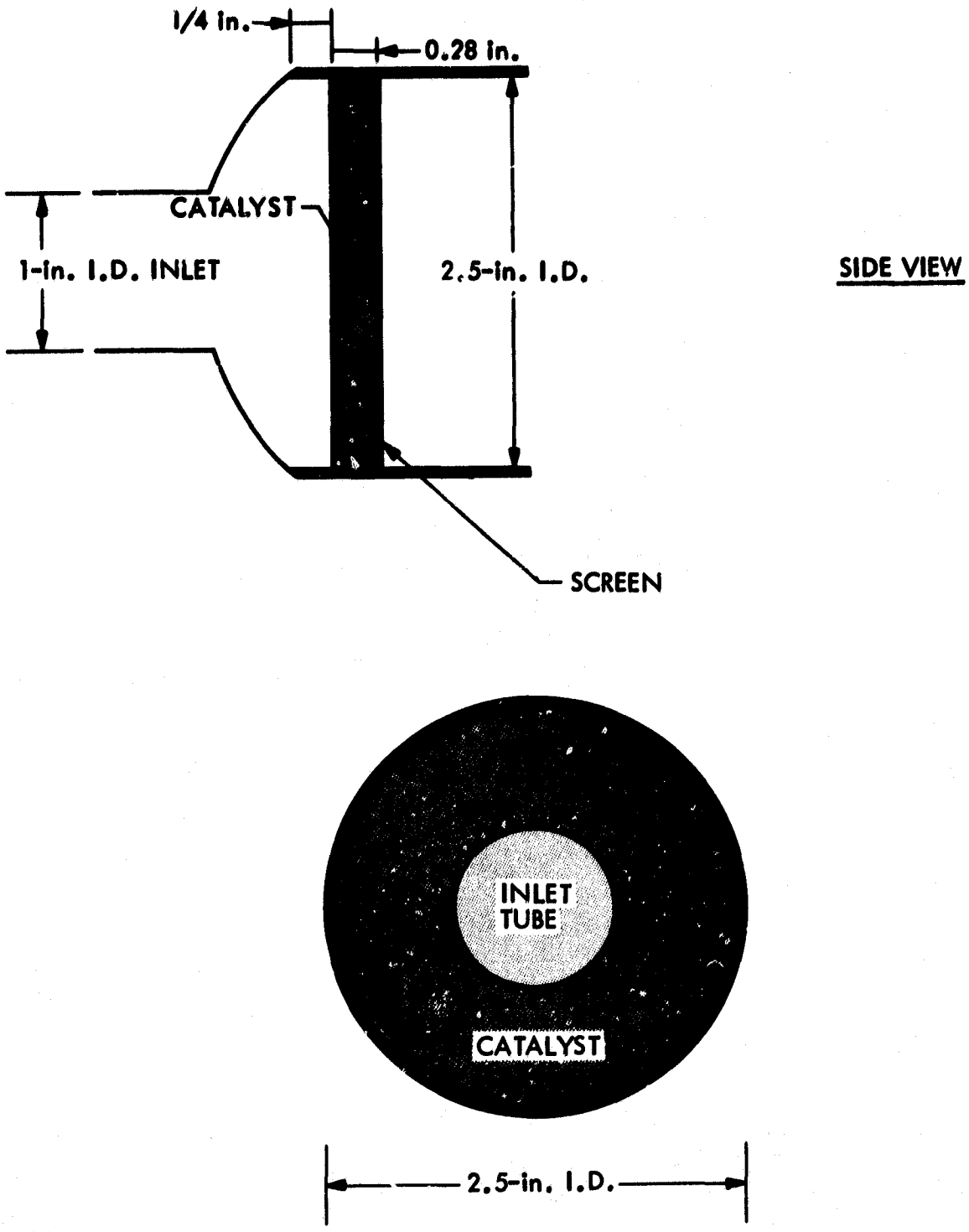

Figure 3-9. Packed Bed Reactor Design Sketch

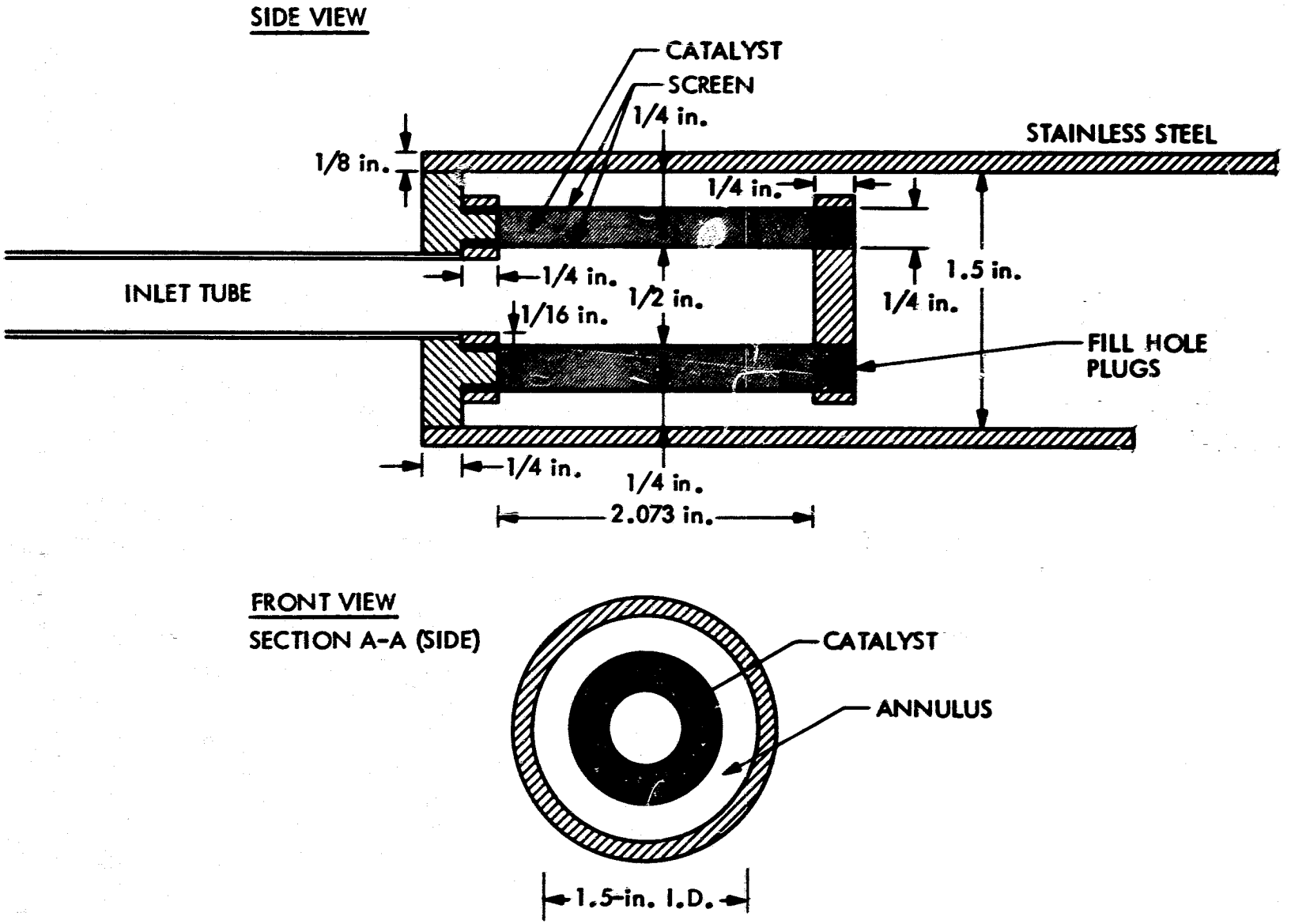

Figure 3-10. Radial Flow Reactor Design Sketch

REFERENCES

2-1 Nast, T. C., Bell, G. A., and Wedel, R. K., "Orbital Performance of a Solid Cryogen Cooling System for a Gamma Ray Detector," Advances in Cryogenic Engineering, Vol. 21, 1976, pp 435-442.

2-2 Pogson, J. T., MacGregor, R. K., "A Method of Increasing the Lateral Thermal Resistance of Multilayer Insulation Blankets," AIAA 8th Aerospace Sciences Meeting, Paper No. 70-15, Jan. 1970.

2-3 Bell, G. A., Nast, T. C., and Wedel, R. K., "Thermal Performance of Multilayer Insulation Applied to Small Cryogenic Tankage," Advances in Cryogenic Engineering, Vol. 22, 1977, pp 272-282.

2-4 Keller, C. W., Cunnington, G. R. and Glassford, A.P., "Final Report - Thermal Performance of Multilayer Insultions," NASA CR-134477, Apr 1974.

2-5 Foster, W. G., Naes, L. A., and Barnes, C. B., "Thermal Conductivity Measurements of Fiberglas Epoxy Structural Tubes from 4K to 320K," AIAA Paper 75-711, May 1975.

3-1 LMSC-D085818. CLIR Cooler Components Definition Study, Nov. 30, 1979.

3-2 Scott, R. B., Cryogenic Engineering, D. Van Nostrand Co., Inc., Princeton, 1959, p 289.

3-3 Bonhoeffer, K. F., Farkas, A., Trans. Faraday Soc., 28, 242 (1932)

3-4 Rudham, R., Tullett, A. D., and Wagstaff, K. P., J. Catalysis, 38, 488-90 (June 1975).

3-5 Brown, D. E., Eley, D. D., and Rudham, R., J. Catalysis, 16, No. 3, 292-302 (1970).

3-6 Kubicka, H., J. Catalysis, 20, No. 2, 163-71 (Feb. 1971).

3-7 Eley, D. D., Forrest, H. and R. Rudham, J. Catalysis, 34, 35-40, (1974).

3-8 Frackiewicz, A., J. Catalysis, 40, No. 2, 184-9, (Nov. 1975).

3-9 Eley, D. D. and D. Shooter, J. Catalysis, 2, 259-73 (1963).

3-10 Weitzel, D. H., Draper, J. W., et al., Advances in Cryogenic Engineering.

3-11 Singleton, A. H., Lapin, A. and L. A. Wenzel, Advances in Cryogenic Engineering, Vol. 13, 409-27-1967.

3-12 Wakao, Smith and Selwood, J, J. Catalysis, 1, p 62-73 (1962).

3-13 Singleton, A. H. and A. Lapin, Advances in Cryogenic Engineering, Vol. 11, 617-30, 1965.

3-14 Singleton, A. H., et al, Technical Documentary Report No. APL-TDR-64-45; June 1964.

3-15 Ergun, S., Chem. Engr. Prog. 48, 89, 1952.